EEG Phase Slips Reveal Detailed Brain Activity Patterns of Novice Vipassana Meditators During Decision Making Tasks

Ratna Jyothi Kakumanu[1¶], Ajay Kumar Nair[2¶], Arun Sasidharan[3], Rahul Venugopal[3], Ravindra P Nagendra[3]*, Bindu Kutty[3], Ceon Ramon[4, 5]*

1. Innovation Incubator Inc., Manhasset Hills, NY 11040, USA
2. Center for Brain and Mind (CBM), Department of Psychiatry, National Institute of Mental Health and Neuro Sciences (NIMHANS), Bengaluru, Karnataka, India.
3. Center for Consciousness Studies (CCS), Department of Neurophysiology, National Institute of Mental Health and Neuro Sciences (NIMHANS), Bengaluru, Karnataka, India
4, 5 Department of Electrical and Computer Engineering[4] and Regional Epilepsy Center[5], University of Washington, Seattle, WA 98195, U.S.A.

Ratna Jyothi Kakumanu	jyothi.maanu@gmail.com	ORCID: 0000-0003-3918-2772
Ajay Kumar Nair	ajay.nimhans@gmail.com	ORCID: 0000-0003-3892-6979
Arun Sasidharan	arunsasi84@gmail.com	ORCID: 0000-0001-7090-2315
Rahul Venugopal	rahul.nimhans@gmail.com	ORICID: 0000-0001-5348-8845
Ravindra P Nagendra	ravindrapinna@gmail.com	ORCID: 0000-0002-8243-8684
Bindu Kutty	bindu.nimhans@gmail.com	ORCID: 0000-0001-7483-9675
Ceon Ramon	ceon@uw.edu, ceon@u.washington.edu	ORCID: 0000-0001-8675-613X

* Corresponding authors for publication: Ravindra P Nagendra, Ceon Ramon
* Corresponding author for review: Ceon Ramon. ceon@uw.edu, ceon@u.washington.edu

¶ These authors contributed equally to this work

Short Title: EEG phase slips for Novice Vipassana Meditators

Preprint available at bioRxiv. doi: https://doi.org/10.1101/2025.09.03.674031

The original document was written in WordPerfect, and a copy was saved in MS Word format. There are some formatting issues with equations in MS Word. Please refer to the original document in PDF for correct formats, line numbers and equations.

	yyyy-mm-dd	
Revision 0:	2025-09-05	(Original submission to bioRxiv)
Revision 1:	2025-10-8	(Revision 1 submission to bioRxiv)

Abstract

Our study adopted a novel approach, utilizing four biomarkers, namely EEG potentials, their first-order derivatives, and phase slip rates derived from each, to discern the differences between novice Vipassana (NVP) subjects and non-meditator controls (NMC). Phase slip rates are discontinuities in instantaneous phase that represent cortical phase transitions, indicating a significant change in the overall brain state. We employed 128-channel EEG data from eight NMC and eight NVP subjects, collected during a gamified protocol, to investigate object identification within a visual oddball paradigm. EEG was continuously acquired during the 50 trials for each subject. We retained 44 artifact-free trials per subject (the minimum common across all subjects) and computed within-subject averages. The EEGs were then averaged separately for NMC and NVP subjects. The EEG was filtered in the alpha band, and the phase was extracted using the Hilbert transform, unwrapped, and the phase slip rates were computed. A montage layout of electrodes was used to make the spatiotemporal plots of biomarkers. Our findings revealed that the spatiotemporal profiles of all four biomarkers differed significantly between the two groups of subjects. Furthermore, the NVP subjects demonstrated faster object recognition. These results not only provide a unique method to use phase slip rates to quantify cognitive differences between NMC and NVP subjects but also present a promising set of biomarkers for quantitative task-based EEG analyses.

Keywords: EEG phase slips, Cortical Phase Transitions, EEG derivatives, Vipassana EEG, Phase Slip Biomarkers, Meditation.

61 **Abbreviations**

62

63 EEG	Electroencephalogram or Electroencephalography
64 EEG′	First order derivative (*d/dt*) of EEG
65 NMC	Non-Meditator Controls
66 NVP	Novice Vipassana
67 RDM*	Relative Difference Measure
68 PSR	Phase Slip Rate or Phase Slip Rates
69 PSR1	Phase Slip Rate extracted from EEG
70 PSR2	Phase Slip Rate extracted from EEG′
71 Poststimulus+	Combined duration of stimulus and poststimulus period

72

73

74 **A. Introduction**

75

76 Phase slips derived from the EEG have been extensively studied to understand cortical
77 neurodynamics under various conditions. These conditions include visual object naming tasks,
78 insight moments [1], dynamics of epileptic seizure evolutions [2], and the formation of
79 propagating spatiotemporal phase cone structures on the cortical surfaces [2, 3]. In all of these
80 studies, there is often additional information about the cortical activity not seen in the power
81 spectral density or phase synchronization analysis of EEG data. Our objective in the present
82 study is to investigate whether additional information can be derived from phase slips extracted

from the EEG of meditative subjects, particularly for novice Vipassana (NVP) subjects in decision-making tasks. Our results indicate that this approach is feasible, offering a promising avenue for future research in meditation and EEG data analysis.

Phase slips are generally extracted from the EEG data using Hilbert transform techniques. However, we have recently demonstrated that these phase slips can also be extracted from the derivatives of EEG data [4], which provides additional information about cortical neurodynamics compared to the phase slips extracted from EEG alone. Here we have written the first order derivative (d/dt) of EEG as EEG′. The phase slip rates extracted from EEG are written as PSR1, and those extracted from EEG′ as PSR2. In the present study, we examined the spatiotemporal behavior of four quantities, viz., EEG, EEG′, PSR1, and PSR2 of novice Vipassana (NVP) meditation subjects and compared them with the spatiotemporal behavior of non-meditator control (NMC) subjects. Our results indicate there are quantifiable differences between NMC and NVP subjects. In addition, we examined the different stages of visual object recognition between NMC and NVP subjects, as well as the time it takes to recognize an object. A detailed analysis of N1, P1, and P2 visual evoked potentials [5] and their corresponding phase slip rates was performed, and there were noticeable differences between NMC and NVP subjects. The insight moments are also called ‘Eureka’ moments when one recognizes an object or spontaneously finds a solution to a problem [1, 6]. To our knowledge, these results are new and open a new way to quantify the effects of meditation on cortical neurodynamics by use of biomarkers based on phase slip rates, such as PSR1 and PSR2.

In the following sections, we provide a brief overview of the necessary background material on cortical phase transitions, phase slips, Vipassana meditation, and insight moments, which will help clarify our methods and results. Details of the methods, results, and discussions are presented in the subsequent sections.

B. Background Material

B.1 Criticality, Phase Transitions, and Phase Slips

Criticality refers to the condition of a system that is finely balanced between order and disorder such that a small perturbation can yield large effects [7]. The sudden large shift in the state of the system is called a phase transition. An example of the critical point is the triple point (273.16 Kelvin, 611.73 Pascal) of water, where it can exist in all three phases of solid, liquid, and gas, and a slight change in the temperature or pressure could cause a shift from one state to the other, e.g., from solid to liquid, etc. Other examples of criticality and phase transitions in nature include superconductivity, ferromagnetism, neuronal activity, and swarm technology [8, 9]. Another typical example of self-organized criticality is the sandpile model [10, 11], where one continually adds sand to a vertical pile until it collapses, triggering cascading avalanches.

Phase slips are discontinuities in rhythmic activity [12, 13] and arise due to the shift from the coordinated synchronous rhythmic activity to more independent asynchronous firing of a group of neurons in the cortex. This generally happens at mesoscopic scales in the brain, but could also

occur at larger interconnected areas in the whole brain. The short (i.e., local) and the long (i.e., global) range electrical interconnections in the brain happen over the white matter fiber pathways. Due to these interconnected regions, one can observe phase slips in the invasive ECoG (Electrocorticogram) recordings and noninvasive EEG (Electroencephalogram) recordings. These phase slips represent cortical phase transitions, indicating a significant change in the overall brain state. These changes in brain states could be related to cognitive processes, such as learning or memory, or changes in internal or external stimuli [1, 13]. Examples of internal stimuli include a shift in attention or a change in an internal thought process. Examples of external stimuli include audio or visual stimuli, temperature, pressure, or even social interactions. All of these could cause a phase transition leading toward the formation of a phase slip.

Phase transitions in the brain occur because the electrical activity of the whole cortex is generally in a metastable state, very close to a critical point, and a slight disturbance could cause a phase transition [14, 15]. The phase transitions produce bursts of neural oscillations, which show up as small perturbations in the EEG, MEG, or ECoG data, which becomes a site for the formation of phase slips. Most of these behaviors of criticality in nature can be modeled with an Ising model of ferromagnetism, which has also been applied to the modeling of avalanches in networked neurons [16]. Some other models based on nonlinear many-body field dynamics have also been proposed for the formation of phase slips at mesoscopic scales in the brain [13, 17, 18]. Thus, in summary, one can consider phase slips as a reliable biomarker to study brain behavior, which has been applied to study the cognitive behavior of the brain from EEG [1] and localization of epileptogenic sites from ECoG [3] and EEG [19] data. In the present report, we are applying

149 these phase slip techniques to study the cognitive behavior of novice Vipassana subjects during
150 decision-making processes.
151
152 **B.2 Vipassana Meditation and Brain Processes**
153
154 Vipassana meditation, as outlined in the Pāli Canon, is rooted in the direct experience of the
155 Buddha and the precise method he used to attain enlightenment. As such, it occupies a central
156 place in Buddhist teachings. Vipassana is a comprehensive system of mental cultivation and a
157 transformative process aimed at elevating consciousness [20]. In contemporary neuropsychology,
158 Vipassana is often equated with "mindfulness" and has been widely adopted as a clinical
159 intervention for managing emotional distress, maladaptive behaviors, and psychosomatic
160 conditions [21]. An expanding body of research highlights its efficacy in enhancing
161 psychological and physical well-being [22, 23], making it one of the most extensively studied
162 psychotherapeutic practices globally. The practice has attracted increasing interest in
163 neuroscience for its potential to foster cognitive flexibility, emotional regulation, and
164 psychological resilience [24, 25].
165
166 Despite the growing empirical interest, many studies have neglected the underlying philosophical
167 context of meditation and its broader implications for consciousness and well-being [26].
168 Moreover, existing research often centers on Western adaptations of Vipassana. Studies on
169 incarcerated populations completing the traditional 10-day courses have found reduced
170 recidivism, depression, anxiety, hostility, and substance use [27]. Studies among experienced

171 Vipassana practitioners in the classical tradition of Sayagyi U Ba Khin, as taught by S.N.
172 Goenka, have identified proficiency-specific psycho-neural correlates of well-being [28, 29].
173 This tradition aims at a radical transformation of consciousness through a sequence of three
174 interdependent meditative techniques designed to accommodate a wide range of temperaments
175 while maintaining internal coherence (Fig. 1).
176
177 ----------
178 **Fig. 1. Vipassana Meditation.** Schematic representation of the Vipassana practice in the
179 tradition of Sayagyi U Ba Khin as taught by S.N. Goenka.
180 ----------
181
182 The training begins with Ānāpāna Sati (Focused Attention Meditation), in which attention is
183 anchored to the breath. This practice cultivates sustained attention, heightened awareness, and
184 perceptual acuity while reducing habitual mind-wandering [30].
185
186 Next, during Vipassana Bhāvanā (Insight Meditation, Mindfulness or Open Monitoring
187 Meditation), practitioners learn to experience the phenomena within the mind-body continuum
188 with objective awareness. These phenomena, including thoughts and feelings, both pleasant and
189 unpleasant, are seen as transient, insubstantial, and ultimately dissatisfactory. Through this
190 sustained, non-reactive observation, the practitioner gains direct insight into the impermanent
191 and impersonal nature of phenomena. Over time, one learns to disidentify from habitual

responses of craving and aversion, seen as sources of suffering, and begins to experience increasing inner stability and self-mastery [30, 31, 32].

Finally, Mettā Bhāvanā (Loving-Kindness/Compassion Meditation) involves the deliberate cultivation and radiance of goodwill toward oneself and all beings, free from bias or reservation. This phase helps dissolve self-centered patterns and reinforce the equanimity gained through Vipassana, supporting the integration of insight into daily life [30]. Throughout Mettā practice, the practitioner maintains an objective stance, extending compassionate awareness without expectation.

These three practices are not discrete but are interwoven, each reinforcing the others in a unified framework for inner transformation [33]. Taken together, they engage cognitive, affective, attitudinal, and ethical dimensions, forming a deeply introspective and socially relevant practice [20].

B.3 Insight Moments and Visual Evoked Potentials

Insight moments are also called 'Aha!' or 'Eureka' moments, which relate to suddenly or spontaneously finding a solution to a problem. A well-known example is the famous ‘Eureka' moment of Archimedes. The ‘Eureka' moment is part of the four stages of creativity suggested by Graham Wallas in 1926, which are commonly called: Preparation, Incubation, Illumination, and Verification [34, 35, 36]. Illumination is the ‘Eureka' moment. These insight moments can be

studied with EEGs, either in the resting state or in evoked response potentials studies, such as looking at a picture on a computer screen while collecting the EEG data [1, 6, 37, 38, 39].

The prominent peaks of visual evoked potentials, P1, N1, and P2, are integral to insight moments, which are generally observed within the first 300 ms from the start of the stimulus onset. After that, within the 0.3 s to 1.2 s time frame from the stimulus onset, several other prominent peaks are also related to different stages of insight moments, allowing the subject to recognize the name, shape, and form of the object on the computer screen and compare them with what is stored in the subject's memory [1]. Thus, analysis of spatial profiles of EEG and phase slip rates for these peaks and their differences between NMC and NVP subjects is an important topic of investigation. An interesting observation from our results was that there was no remarkable difference in the latency of P1, N1, and P2 peaks for the NMC and NVP subjects. However, there were some noticeable differences in the spatial profiles of these peaks for NMC and NVP subjects. More details are given in the results section.

C. Materials and Methods

C.1 Participants

High-density EEG data of 16 healthy adult participants (8 NMC, 8 NVP) were used in this study. No new data sets were collected for this study. We conducted secondary data analyses on a subset of EEG data previously collected in prior projects [28, 29], where details of the data

acquisition protocols and participant characteristics have been described. In brief, NMC participants (n=8, 4 females) were in the age range of 23 to 57 years with an average age of 37.6±10 years. For the NVP participants (n=8, 7 females), the age range was 29 to 60 years with an average age of 48.5±10 years. NVP participants had an average meditation experience of 2.2 years with a maximum experience of 3.0 years. The average meditation hours were 1,080. The NMC participants had no prior experience with meditation. These details are also summarized in Table 1.

Table 1. Participant groups' mean age and estimated hours of meditation experience.

	NMC (n=8)	NVP (n=8)
Age (years)	37.6±10	48.5±10
Gender (female/8)	4	7
Meditation hours	0.0	1080.0

The inclusion criteria were: NVP participants should have completed two or three ten-day courses in Vipassana meditation with less than three years of practice and no exposure to any other form of meditation. NMCs should have had no exposure to any form of meditation. All had basic literacy in at least one language: English, Hindi, or Kannada. The exclusion criteria were: participants with neurological or psychological disorders, a history of substance abuse, or on psychiatric or neurological medications. These exclusion criteria were chosen to ensure that the participants' EEG data were not influenced by any external factors that could impact their brain activity, thereby maintaining the integrity of the study.

262 Participants were recruited with permission from the Vipassana Research Institute (VRI),
263 Igatpuri, India, via study pamphlets and VRI newsletter advertisements at Vipassana training
264 centers across India. Non-Meditating controls were recruited from the local community in
265 Bangaluru, India. All participants volunteered to participate in the study. Food, accommodation,
266 and travel expenses were offered, along with no other form of financial incentives.
267
268 All participants provided written informed consent, which was obtained after a detailed
269 explanation of the study's purpose, procedures, and potential risks and benefits. The NIMHANS
270 Institute's Human Ethics Committee approved the consent process, which was in accordance with
271 the Declaration of Helsinki (1964). The study took place at the Human Cognitive Research
272 Laboratory in the Department of Neurophysiology, NIMHANS, Bengaluru, India. Participants
273 had at least a high school education, and the majority belonged to the middle-income category, as
274 defined by Indian standards. Participants were all healthy, right-handed, non-smokers and
275 refrained from any caffeinated beverages on the day of the study.
276
277 Although the meditators were recruited from all over India and were practicing a standard form
278 of meditation, no systematic sampling approach, such as cluster sampling, was used to obtain a
279 representative national sample. However, our selected participants represent a typical sample of
280 the educated middle class who may practice Vipassana meditation. As meditation has become a
281 global phenomenon in today's world, our sample would also represent the trends of modern
282 society in various parts of the world. This global relevance extends to the non-meditating control
283 samples in the middle-class society of India and worldwide.

C.2 EEG Data of Subjects

A 128-channel EGI system (Electrical Geodesics, Inc., Eugene, OR, USA; now part of Magstim Inc., 1626 Terrace Dr, Roseville, MN 55113) was used for the data collection. Details on the task parameters have been previously reported [40]. In brief, participants engaged in 'ANGEL', a gamified audiovisual oddball task with three levels of complexity, presented in 16 blocks each. The first two blocks of data from the second level ('Whodunnit'), comprising of 50 trials were used for the present study. Each block had a salient image (black and white face, shape, or a distorted image) presented on one side of a fixation sign, and a non-salient image (black and white checkerboard) presented on the other side. Further, images of one salient image type were presented frequently on one side in a block (for example, a face presented on the right of the fixation) and represented the 'frequent' condition. About 20% of the time ('rare' trial condition), a salient image of one of the other three image types was presented on the other side (for example, shape to the left of the fixation). Participants were asked to press one of two buttons to indicate if the salient image appeared on the left or the right of the fixation. Figure 2 shows an example of the sequence of images.

Fig. 2. Audiovisual oddball task. Protocol Diagram from earlier publication. Representative examples of two types of task blocks. (From Nair et al., 2016).

---

306 **C.3 Preprocessing of the EEG Data**

307

308 We used MATLAB (MathWorks Inc., Natick, MA, USA) and EEGLAB software 41] for
309 preprocessing the EEG data, phase slip computations, and visualization of results. The data was
310 filtered with an equiripple filter in a 3–49 Hz broadband and then re-referenced to the common
311 averaged reference. The upper frequency of 49 Hz was selected to eliminate the contamination
312 from the power-line frequency of 50 Hz in India, where the data sets were collected. Using the
313 ICA (independent component analysis) techniques, the muscle, eyeblink, and heartbeat artifacts
314 were removed. After that, the data were averaged over trials for each subject. For one subject, we
315 found 44 good trials out of 50. For consistency, we chose 44 good trials out of 50 for all subjects.
316 The averaged trials for eight NMC and eight VPN subjects were averaged. This way, at the end,
317 we had one grand-averaged data set for NMC subjects and another similar data set for NVP
318 subjects. These data sets were then again referenced to the common averaged reference for each
319 channel, filtered in the alpha (7–12 Hz) band with an equiripple filter, and then used for phase
320 slip extraction and PSR computations.

321

322 An example of the EEG data after preprocessing is shown in Fig. 3. It is only for two electrodes,
323 one in the frontocentral area (Fig. 3A) and the other in the right visual area (Fig. 3B). Their
324 spatial location is shown in Fig. 3C. The periods of prestimulus, stimulus, and poststimulus
325 period are marked on the top of the EEG plot in Fig. 3A. For analysis and display the time scale
326 for the prestimulus period is -1.0 s to 0.0 s, for the stimulus period is from 0.0 s to 0.240 s, and
327 for the poststimulus period is from 0.240 s to 2.0 s, respectively. The prestimulus period is also

commonly referred to as the baseline period. Additionally, we use the terminology 'poststimulus+' to refer to the combined duration of the stimulus and poststimulus period from 0.0 s to 2.0 s.

Fig. 3. EEG traces and spatial profiles. An example of an EEG trace after preprocessing for two electrodes in a 3-49 Hz broadband. (A) EEG from one of the electrodes in the frontocentral area, (B) EEG from one of the electrodes in the right visual area, and (C) spatial profile of EEG potentials at the P1 peak of the NVP subject. Note that the time series profiles of PSRs at two electrodes are significantly different during the 0.0-1.0 s period, when the subject is visualizing and analyzing the image of the object during covert object naming tasks.

The EEG plot of the right visual electrode (Fig. 3B) has three prominent peaks marked as P1, N1, and P2, which are typical visual event-related potentials [5] observed when one begins to look at an object. It is part of the perception cycle during the stimulus period. The same peaks are also marked in Fig. 3A for the frontocentral electrode. Notice that the polarity of the peaks is reversed in Fig. 3A compared to Fig. 3B. For simplicity, we will use the positive and negative nomenclature of the peaks from the visual electrode in Fig. 3B.

An interesting feature is that these peaks for NMC and NVP subjects are very close. This would suggest two things. First, our data collection and stimulus protocol are robust, so the data collected over several days does not smear the prominent peaks in the EEG data. The second point is that the initial response of the brain to a visual stimulus is very similar in NMC and NVP subjects. For the NVP subjects, these P1, N1, and P2 peaks are located at 115 ms, 214 ms, and 303 ms, respectively, from the start of the stimulus period at 0.0 s. The location of these peaks for the NMC subjects is at 122 ms, 190 ms, and 305 ms, respectively. More details about these peaks are given in the Results section.

During the period of 0.4 to 1.0 s, several prominent peaks with different locations are observed for NMC and NVP subjects. These peaks correspond to the various stages of insight moments [1, 37] related to decision-making and object recognition processes, such as searching for the name and form of the object in memory [1]. These insight moments can be studied during both the stimulus period [6] and/or during the poststimulus period [1, 42, 43]. A detailed analysis of these insight moments for NMC and NVP subjects is given in the Results section.

A note about the spatial plot in Fig. 3C, which will also apply to subsequent spatial plots. The head circle represents the largest possible diameter of the head, as seen from the top, and it covers most of the electrodes on top of the head, positioned slightly above the level of the eyebrows. In addition, there are several lower-level electrodes positioned around the head, which are located below the eyebrows and extending down to ear level. The electrical activity on these electrodes is shown outside the head circle. These electrodes will pick up the electrical activity of

the sources in the temporal areas, as well as from the lower, i.e., inferior, and deeper parts of the brain, such as the amygdala, based on the orientation of the sources. There are some electrodes on the forehead, whose electrical activity will be included outside the head circle above the nose in spatial plots. A few of the electrodes on the face are not included in the spatial plots. More details about this can be inferred from the topographic plot script (topoplot.m) included in the EEGLAB software.

C.4 Phase Slip Rate Computations

The procedures to compute PSR are described in our previous studies [1, 4]. Similar procedures have been used here. The sawtooth patterns of the phase were extracted from the EEG data using the Hilbert transform, which, on unwrapping and detrending, shows phase slips at the locations of small perturbations in the EEG data related to cortical phase transitions. A pictorial representation of phase slip extraction from EEG and its first derivative is given in Fig. 4. It shows the EEG and its first order derivative, EEG′ from one of the electrodes in the front central area, sawtooth pattern of the phase, unwrapped phase with one of the large episodic phase shifts, and several of the large sharp and small broad phase slips. Our interest will be only in the phase slips in the alpha band of 7-12 Hz, and, thus, larger phase slips will not be counted in PSR computations. The PSR1 is from the EEG, and the PSR2 is from the first derivative of the EEG, respectively. Here, EEG voltage is represented as a time series data: $y = y_1 + y_2 + ... + y_n$, and y' is (dy/dt) of the time series. The y' was computed by the first order differencing of the time series

392 *y* and then dividing it by the digitization interval. A similar representation has been used earlier
393 [4, 44].
394
395 ---
396 **Fig. 4. A pictorial representation of the phase slip extraction steps.** Plots in the left column
397 are marked in (A) for the phase slips extraction from the EEG, and, similarly, the right
398 column (B) is for the phase slips extraction from EEG′, i.e., from the first order
399 derivative of EEG. The top row is the EEG and EEG′, the second row from the top is the
400 sawtooth pattern of the phase, the third row from the top is the unwrapped phase, and the
401 bottom row shows some of the phase slips.
402 ---
403
404 The PSR from the phase slips was calculated in a stepping window of 10 ms duration with a step
405 size of one digitization point equal to 1.0 ms based on the sampling rate of 1 kHz. The window
406 size is selected based on the Shanon entropy function [45, 46, 47] such that it is short enough to
407 capture the information (lower entropy) but not wide enough to smear (higher entropy) the
408 information. For our case, a window size of 10 ms will give us a maximum value of PSR of 10
409 counts/10 ms if there were phase slips at each digitization point. In general, it will be difficult to
410 find phase slips at each digitization point, and thus, PSR will be less than 10 counts in each
411 window. The step size of one digitization point, i.e., 1.0 ms, is 10% of the window size, which
412 provides smooth transitions without smearing the information content in going from one stepping
413 window to the next. Also, this window size is approximately 7% of the time period of the lowest

414 frequency (7 Hz) of interest in the alpha band, and the step size is adequate to avoid aliasing
415 errors due to undersampling.
416
417 These procedures were used for computing phase slip rates, PSR1 from the EEG data, and PSR2
418 from the first order derivative of the EEG data. The spatial plots of EEG, PSR1, and PSR2 were
419 constructed with a montage layout of 128 electrode positions on a flat surface.
420
421 To separate the phase slips arising from the biological processes versus the random noise, several
422 criteria were applied, which we have used before [4]. These include: (1) phase slip frequency is
423 within the alpha band of 7–12 Hz, (2) sign of the positive or negative peaks did not change for at
424 least three consecutive time steps, and (3) the magnitude of the three consecutive peaks was
425 within the mean ± 1.05σ of the three peaks, where σ is the standard deviation of the mean. The
426 application of these criteria significantly reduced the counting of phase slips due to random
427 noise, while simultaneously maximizing the counting of phase slips from biological processes.
428
429 **C.5 Surrogate Data Testing**
430
431 After filtering in the alpha band, the PSR of random noise was computed from the randomly
432 shuffled EEG data. We used the 'randperm' command in the MATLAB software for this. These
433 techniques have been used before by us [1, 2, 4] and also described in a recent paper [48] on
434 surrogate data analysis. The power spectral density of the randomly shuffled EEG data was
435 significantly different from the original EEG data, and it was close to a white noise. The phase

slips were extracted from the randomized EEG data and then randomly shuffled. After that, the PSR1 was computed in a stepping window of 10 ms duration with a step size of one digitization point. The mean and standard deviations of PSR1 were found to be zero after averaging over n = 100 trials. A similar analysis was also performed on the PSR2 derived from the first order derivatives of the randomly shuffled EEG data. It was found that in this case also, the mean and standard deviations of PSR2 from the shuffled data were zero after averaging over n = 100 trials. This shows that our reported results are from the biological processes extracted from the EEG data and are above the results from the random noise.

C.6 Statistical Analysis

To compare two data sets, we used a paired Student's t-test or histogram distributions. However, these two tests often fail if the means and standard deviations of two distributions are very close to each other. Similarly, the Kolmogorov-Smirnov test also fails if two cumulative distribution functions are similar, even though there are observable and quantifiable differences in their spatial plots. In such situations, the Relative Difference Measure (*RDM**) and the Magnification Factor (*MAG*) are considered to be better choices than the Student's t-test, the Kolmogorov-Smirnov test, or the histogram distribution to compare two spatial plots of similar values [2, 45]. It is a prevalent technique to quantify the differences between two spatial plots of data, such as in EEG spatial plots [2, 45]. Most of our results are spatial plots of EEG or phase slip rates. The *RDM** is defined as:

$$RDM^* = \sqrt{\sum_{j=1}^{m}\left[\frac{Z_k^{RM}}{\sqrt{\sum_{k=1}^{m}\left(Z_k^{RM}\right)^2}} - \frac{Z_k^{TM}}{\sqrt{\sum_{k=1}^{m}\left(Z_k^{TM}\right)^2}}\right]^2} \quad \textbf{(1)}$$

where index, $j=1:m$, runs over all 128 electrodes. The Z_k^{RM} are the values for the reference measurement, and Z_k^{TM} are the values of the test measurements. As an example, it could be the EEG potential at the kth electrode for the reference measurements (RM) and the test measurements (TM), respectively. The magnification factor is defined as:

$$MAG = \frac{\sqrt{\sum_{k=1}^{m}\left(Z_k^{TM}\right)^2}}{\sqrt{\sum_{k=1}^{m}\left(Z_k^{RM}\right)^2}} \quad \textbf{(2)}$$

The *RDM** is a measure of the difference in spatial profiles of two data sets, and *MAG* is a measure of differences in the magnitude of the two data sets. If two data sets are the same, *RDM** will be zero and *MAG* will be unity. The degree of differences is quantified with higher values of *RDM** in the range of 0.0 to 1.0. The maximum value of *RDM** is 1.0 if the test measurements are zero. The variation in the value of *MAG* from unity will quantify the differences in the magnitude of the two data sets. Values of *MAG* greater than 1.0 would mean that the test measurements (TM) are higher in magnitude as compared with the reference measurements (RM). And the reverse is true if *MAG* is less than 1.0.

To compare the means of more than two data sets, we used ANOVA (Analysis of Variance). Histogram plots of data sets were also made. Mean and standard deviations of two histogram plots were computed and compared. In addition, two histogram distributions were also compared with their RMS bin count differences, $RMS\ H_{diff}$, defined as:

$$RMS\ H_{diff} = \sqrt{\frac{1}{N}\sum_{i=1}^{N}((H_1(i) - H_2(i))^2} \qquad \textbf{(3)}$$

where H_1 and H_2 are two histogram distributions with N bins.

C.7 Computational Resources

The data analysis was performed on a desktop computer with an 8-core CPU and 112 GB of memory using EEGLAB [41]. For computations of PSR requiring more significant (>112 GB) memory, we used MATLAB software at the UCSD (University of California, San Diego) supercomputing center using their NSG (Neuroscience Gateway) portal.

D. Results

D.1 Non-meditator Control (NMC) Subjects

The temporal plots of EEG, EEG′, PSR1, and PSR2 of one of the electrodes in the front central area are given in Fig. 5. During the stimulus and poststimulus periods, the prominent

event-related potential peaks are recognizable in the top left plot of broadband EEG in the 3-49 Hz, which are difficult to see in the alpha band EEG plot, (left and right middle plots). The prominent peaks in the EEG are difficult to recognize in the plot of the EEG′ (top right plot). They tend to disappear with the first-order differentiation of the EEG. However, the small high-frequency perturbations in the EEG are amplified due to the removal of linear trends through differentiation. In the alpha band, one can see the presence of the alpha wave spindling and small perturbations in the EEG and also in the EEG′.

Fig. 5. EEG, its derivative, and phase slip rates. Temporal plots of quantities of one of the electrodes in the front central area for non- meditator control (NMC) subjects. (Top left) EEG in 3-49 Hz band, (top right) EEG′ in 3-49 Hz band, (middle left) EEG filtered in the alpha band of 7-12 Hz, (middle right) EEG′ filtered in the alpha band of 7-12 Hz, (bottom left) phase slip rate PSR1 extracted from EEG in the alpha band, and (bottom right) phase slip rate PSR2 extracted from EEG′ in the alpha band. Notice the prominent peaks in PSR1 and PSR2 related to brain activity during the visual object recognition tasks. The prestimulus period is from -1.0 to 0.0 s. The combined stimulus and poststimulus period, referred to as the poststimulus+ period, spans from 0.0 to 2.0 seconds.

The PSR1, computed from the EEG data filtered in the alpha (7-12 Hz) band, provides crucial insights. Notably, the PSR1 plot reveals a small and large peak between -0.9 s and -0.45 s during the prestimulus period. These peaks are associated with the background activity of the brain while looking at the checkerboard pattern during the prestimulus period. The broad peak during the poststimulus period, stretching from 0.15 s to 0.95 s, with the prominent peak centered at 0.6 s, is equally significant. This peak is related to the initial response of the visual cortex and the recognition of the object in the language and memory areas of the brain, a common occurrence in the insight moment analysis of visual object naming [1]. The broad peak between 1.35 and 1.9 s is probably related to the brain returning to the background activity after the end of visual object naming processes.

The plot of PSR2 reveals the rate of change in the neuronal population participating in the formation of scalp EEG. It exhibits a bifurcated peak between -0.8 and -0.2 s during the prestimulus period, which correlates with the background activity of the brain while viewing the checkerboard pattern. During the first second of the combined stimulus and poststimulus period, a broad peak is observed from 0.0 to 0.8 s, with the main peak at 0.45 s, which is likely related to the recognition of the object in memory and language areas [1, 37]. The several peaks from 1.0 s to 2.0 s correspond to the return to background activity.

The spatial plots of the root mean square (RMS) of EEG and EEG′, and mean values of PSR1 and PSR2 for NMC subjects are given in Fig. 6. These values were computed within a stepping window of 0.5 s covering the period of -1.0 to 2.0 s.

Fig. 6. Plots of EEG and PSR of non-meditator control (NMC) subjects. Spatiotemporal plots of the root mean square (RMS) values of EEG and its first order derivative (EEG′) and their associated mean values of phase slip rates for non-meditator control (NMC) subjects. The RMS and mean values were computed within a 0.5 s stepping window. The temporal duration for each frame is given at the top. (A) The top two rows are for the RMS EEG and the mean PSR1, respectively. (B) The bottom two rows are for the RMS EEG′ and the mean PSR2. Notice the shifting spatial patterns of all four quantities.

Fig. 6 is divided into sections (A) and (B). The top two rows in section (A) present the spatial plots of RMS EEG and the mean values of associated phase slip rate, i.e., mean of PSR1 (#/(10 ms)), respectively. The RMS and mean values were computed within a 0.5-s stepping window. Similarly, the bottom two rows marked as section (B) are the spatial plots of the RMS value of the first-order derivative of EEG, i.e., EEG′, and the mean values of its associated phase slip rate, PSR2 (#/(10 ms)), respectively. The frame numbers and their temporal durations are given at the top. The first two frames, i.e., Frame 1 and Frame 2, are during the prestimulus period. The Frame 3 from 0.0 s to 0.5 s is for the combined period of stimulus (0.0 to 0.240 s) and part of the poststimulus (0.240 s to 0.5 s) period. The remaining three frames are for the poststimulus period.

In all frames, RMS EEG activity is intense in the forehead area above the nasion point, corresponding to the brain activity in the brain's frontal area responsible for the emotional responses to external stimuli, such as visual images on the computer screen. In Frame 1 and Frame 2, it is subdued, begins to increase in Frame 3, and becomes strongest in Frame 4. After that, it starts to decrease in subsequent Frames 5 and 6. There is another activity spot in the left frontocentral area, which is present in all six frames. It is of moderate strength (0.2 μV) during the prestimulus period but becomes stronger during the poststimulus period, with the most substantial value of 0.3 μV in Frame 4. The mean PSR1 plots (Fig. 6A, bottom row) differ from RMS EEG plots. There is a bright spot near the right ear in the central right temporal area. It is present during the stimulus period and also during the poststimulus period. Its activity is noticeable in Frames 3 to 4 during the poststimulus period and almost disappears in Frame 6. There is also an active spot in the right frontocentral area, located just to the right side, below the nose. The activity at this spot is high in Frames 3 and 4, which matches the several peaks of event-related potentials in the EEG during this period (Fig. 5, top left plot). An interesting feature to note is that mean PSR1 activity is widespread in the lower half of the plot, with some areas in the central and parietal regions, as well as others near the left and right edges of the plot. These corresponding features are not visible in the spatial plots of the RMS EEG.

The spatial plots of RMS EEG′ and the corresponding mean PSR2 are given in Fig. 6B. The spatial features in RMS EEG and RMS EEG′ are very similar, which is expected because EEG′ is the first order derivative of the EEG. Similarly, the spatial patterns of mean PSR2 are similar

578 to those of mean PSR1, representing the rate of change of the neuronal population involved in
579 cortical electrical activity.
580
581 A one-way ANOVA analysis was performed on the six frames of RMS EEG, and it was found
582 that the mean of all six frames were significantly ($p < 0.01$) different from each other. A similar
583 analysis was performed on the remaining three quantities, namely, RMS EEG′, mean PSR1, and
584 mean PSR2. Results were similar, i.e., the means of the six frames for each quantity were
585 significantly ($p < 0.01$) different from one another. A comparative analysis of the six spatial plots
586 of EEG and PSR1 was done with the paired Student's t-test, and it was found that each frame was
587 significantly ($p < 0.01$) different from the others. A similar analysis was performed on each frame
588 of RMS EEG′ and the mean PSR2, and it was found that they were significantly ($p < 0.01$)
589 different from each other.
590
591 **D.3 Novice Vipassana (NVP) Subjects**
592
593 All quantities related to one of the frontocentral electrodes for NVP subjects are given in Fig. 7.
594 There are well-defined and recognizable peaks in the EEG during the prestimulus, stimulus, and
595 poststimulus periods. During the prestimulus period, the prominent peaks are located at -0.88 s,
596 -0.793 s, and -0.67 s. These peaks are related to the background activity of looking at the
597 checkerboard pattern on the computer screen. During the stimulus and poststimulus periods, the
598 prominent peaks are at: 0.172 s, 0.4 s, 0.56 s, 0.702 s, and 0.903 s. These peaks are related to
599 insight moments [37] for visualization and recognition of the object during the stimulus and

poststimulus periods [1]. Their temporal location for NVP subjects differs from that of the NMC subjects. This is also reflected in the plot of PSR1. The prominent peaks are at -0.544 s, 0.436 s, 0.65 s, 0.823 s, and 1.503 s. These plots suggest that the timings for the object recognition steps for NVP subjects are slightly different from those of NMC subjects.

Fig. 7. One electrode plot of NVP subjects. Temporal plots of quantities of one of the electrodes in the front central area for novice Vipassana (NVP) subjects. (Top left) EEG in 3-49 Hz band, (top right) EEG′ in 3-49 Hz band, (middle left) EEG filtered in the alpha band of 7-12 Hz, (middle right) EEG′ filtered in the alpha band of 7-12 Hz, (bottom left) phase slip rate PSR1 extracted from EEG in the alpha band, and (bottom right) phase slip rate PSR2 extracted from EEG′ in the alpha band. Notice the prominent peaks in PSR1 and PSR2 related to brain activity during the visual object recognition tasks

---

The spatiotemporal plots of brain activity for NVP subjects are given in Fig. 8. These plots are slightly different from the corresponding plots of NMC subjects. There is a bright spot near the nose in the RMS EEG plot in Frame 1. The activity related to the orbital brain is picked up by the electrodes on the forehead above the nasion point. This disappears in the subsequent frames. In Frame 3, there is a large bright spot at the bottom, which relates to the first impressions of the visual stimulus during the stimulus and the start of the poststimulus period. In the following two

frames, frames 4 and 5, a low level (~ 0.1 μV) RMS EEG activity is spread in the broader area in the left frontal, central, and left central parietal areas. These are probably related to a search for the name and form of the stimulus object in the language and memory areas of the brain. Frame 6 represents the return to the brain's background activity while looking at the checkerboard pattern.

Fig. 8. Plots of EEG, its derivative, and PSR of NVP subjects. Spatiotemporal plots of the root mean square (RMS) values of EEG and EEG′ and their associated mean values of phase slip rates for novice Vipassana (NVP) subjects. The RMS and mean values were computed in the stepping window of 0.5 s duration. The temporal duration for each frame is given at the top. (A) The top two rows are for the RMS EEG and the mean PSR1, and (B) the bottom two rows are for the RMS EEG′ and the mean PSR2, respectively. Notice the shifting spatial patterns of all four quantities from Frame 1 to Frame 6.

The spatial patterns of mean PSR1 plots are different from the RMS EEG spatial plots. This is particularly noticeable in frames 3, 4, and 5 when the bulk of the brain activity happens to recognize the visual stimuli on the screen. The brain activity is widespread in different parts of the brain and becomes less in Frame 5. In Frame 6, the PSR1 activity is similar to that in Frame 1, signifying that brain activity has returned to the background level at the end of the trial. The spatial patterns of RMS EEG and RMS EEG′ are similar. Similarly, the spatial patterns of mean PSR1 and PSR2 are very similar except in Frame 6. The PSR2 activity has two bright spots, one

near the left central temporal area and one in the left posterior area, which are absent in the PSR1 spatial plot.

A one-way ANOVA analysis was performed on the six frames of four quantities, viz., RMS EEG, RMS EEG′, PSR1, and PSR2. It was found that the means of all six frames were significantly ($p < 0.01$) different from each other for each of the four quantities. A comparative analysis of the six spatial plots of EEG and PSR1 shown in Fig. 8 for NVP subjects was performed using the paired Student's t-test, and it was found that each frame was significantly different from the others ($p < 0.01$). A similar analysis was performed on each frame of RMS EEG′ and the mean PSR2, and it was found that they were also significantly different from each other ($p < 0.01$).

D.3 Differences between NMC and NVP Subjects

D.3.1 EEG and PSR1 Differences between NMC and NVP Subjects

The poststimulus+ values above the prestimulus, i.e., baseline values, were computed for the NMC and NVP subjects. For these purposes, the stimulus period of 0 to 240 ms was combined with the poststimulus from 0.24 s to 2.0 s, and it is called the poststimulus+ period. In general, the majority of the brain response happens between 0.04 s and 1.2 s from the start of the visual stimulus at 0.0 s [1]. The RMS EEG was computed for the pre- and poststimulus+ periods separately. Then the prestimulus values were subtracted from the poststimulus+ values to obtain

666 the values above the baseline, i.e., above the prestimulus values. The same procedures were
667 repeated for RMS EEG′, mean PSR1, and PSR2.
668
669 ----------
670 **Fig. 9. Activity patterns above the baseline.** (A) Spatial plots of RMS EEG above the baseline
671 of NMC and NVP subjects, (B) corresponding spatial plots of mean PSR1 above the
672 baseline, (C) histogram distribution of RMS EEG values shown in spatial plots of A, and
673 (D) histogram distribution of PSR1values shown in spatial plots of B.
674 ----------
675
676 RMS EEG and mean PSR1 above the prestimulus are given in Fig. 9. The spatial plots of RMS
677 EEG are shown in Fig. 9A, and the mean PSR1 are given in Fig. 9B. The left plot is for NMC
678 subjects, and the right plot is for NVP subjects. For NMC subjects, the RMS EEG activity is very
679 strong at the top of the plots, which is from the electrodes on the forehead area and near the eyes.
680 We have removed the artifacts related to eye motion and eye blinks; thus, these electrodes likely
681 show the activity from the orbital and frontal lobes of the brain. In comparison, the frontal
682 activity is low for NVP subjects. In addition, for NVP subjects, there is more activity outside the
683 head circle in the left temporal areas. Inside the head circle for NMC subjects, there are bright
684 spots in the frontal and left central regions, which are less intense for NVP subjects. The paired
685 Student's t-test showed a significant ($p < 0.01$) difference between the spatial plots of the RMS
686 EEG of NMC and NVP subjects. Similarly, the RDM* and MAG values of 1.36 and 1.04,
687 respectively, suggest some noticeable differences between the two spatial plots. The RDM* of

1.36 would suggest a 36% difference in spatial distribution. The MAG of 1.04 would indicate that there is a 4% difference in the magnitude between the two plots. This is very much evident in the differences in the relative magnitude of bright spots at similar locations in the two plots. These differences are also visible in the histogram plot of Fig. 9C. The mean values of histogram counts are the same for both groups, but the standard deviations, σ, are different. The RMS values of histogram bin counts for NMC and NVP subjects are 22.33 and 19.49 counts, respectively. The RMS values of histogram bin counts for NMC and NVP subjects are 22.33 and 19.49 counts, respectively. The RMS difference of histogram bin counts, RMS H_{diff} is 17.55 counts. This translates to about a 42% difference for the total bin counts, and could be considered a significant difference between the NMC and NVP subjects.

The spatial plots of PSR1 are given in Fig. 9B, and the corresponding histogram distributions are given in Fig. 9D. For NMC subjects, the mean PSR1 is distributed all over the plot. In contrast, for the NVP subjects, it is strong in the left and right temporal areas. Also, a bright spot near the right ear, which does not have a corresponding high activity in the EEG plot. A paired Student's t-test was performed on the absolute values of mean PSR1 for the NMC and NVP subjects, and it was found that they were significantly ($p < 0.05$) different from each other. The *RDM** and *MAG* values are 1.41 and 1.38, which will also suggest that the two plots are significantly different. The mean values of histogram counts of PSR1 are the same for both groups, but the standard deviations, σ, are different. The RMS values of histogram bin counts of PSR1 for NMC and NVP subjects are 20.74 and 18.88 counts, respectively. The RMS difference of histogram bin counts is 6.52 counts. This translates to about a 16% difference when normalized to the total number of

bins, and could be considered a noticeable difference in the histogram counts of PSR1 between the NMC and NVP subjects.

D.3.2 EEG′ and PSR2 Differences between NMC and NVP Subjects

RMS EEG′, mean PSR2 above the prestimulus values, and their corresponding histogram distributions are given in Fig. 10. For NMC subjects, the RMS EEG′ activity is very strong at the top of the plots, which is from the electrodes on the forehead area and near the eyes. In contrast, for NVP subjects, the RMS EEG′ activity is in the left side temporal regions of the plots. The differences in their spatial distributions are exemplified by the *RDM** value of 1.27, while their magnitudes are very similar, as indicated by the *MAG* value of 1.08. A paired Student's t-test was performed on the RMS EEG′ values for the NMC and NVP subjects, and it was found that they were significantly ($p < 0.01$) different from each other. A histogram distribution of these values are given in Fig. 10C. The mean values of histogram counts are the same for both groups, but the standard deviations, σ, are different. The σ is ±18.56 and ±13.65 for the NMC and NVP subjects, respectively. This translates to about a 26% difference between σ for the NMC and NVP subjects and could be considered a significant difference between the two σ values. The RMS values of histogram bin counts for NMC and NVP subjects are 21.79 counts and 18.21 counts, respectively. The RMS difference of histogram bin counts, RMS H_{diff} is 16.95 counts. This translates to about a 42% difference for the total bin counts, and could be considered a significant difference between the NMC and NVP subjects.

732 ----------

733 **Fig. 10.** **Activity patterns of the first derivative of EEG and PSR2 above baseline.** (A)
734 Spatial plots of RMS EEG′ above the baseline of NMC and NVP subjects, (B)
735 corresponding spatial plots of mean PSR2 above the baseline, (C) histogram
736 distribution of the RMS EEG′ values shown in spatial plots of A, and (D)
737 histogram distribution of PSR2 values shown in spatial plots of B.

738 ----------

739

740 The spatial plots of PSR2 for the NMC and NVP subjects are given in Fig. 10B. For the NMC
741 subject, the hot spots in PSR2 match fairly well with the hot spots in RMS EEG′. However, there
742 are additional hot spots for the NVP subjects in the right parietal areas, which are absent in the
743 RMS EEG′. A paired Student's t-test failed to show any significant differences between the
744 PSR2 values for the NMC and NVP subjects. However, the *RDM** of 1.34 suggests that spatial
745 distributions of PSR2 are significantly different from each other, as shown in Fig. 10B.

746

747 A histogram distribution of PSR2 is given in Fig. 10C. The mean values of histogram counts are
748 the same for both groups, but the standard deviations, σ, are different. The σ is ±11.49 and
749 ±13.10 for the NMC and NVP subjects, respectively. This translates to about a 14% difference
750 between σ for the NMC and NVP subjects. The RMS values of histogram bin counts for NMC
751 and NVP subjects are 16.81 counts and 17.84 counts, respectively. The RMS difference of
752 histogram bin counts, RMS H_{diff} is 5.58 counts. This translates to approximately a 16% difference

753 in total bin counts, which could be considered a slight difference between the NMC and NVP
754 subjects.
755
756 **D.4 Insight Moments of Object Recognition**
757
758 EEG potentials in the broad band (3-49 Hz) and the corresponding phase slip rates in the alpha
759 (7-12 Hz) at one of the electrodes in the right visual cortex are presented in Fig. 11. A choice was
760 made to dispaly EEG potentials in the broad band because the P1, N1 and P2 peaks are easily
761 recognizable which are difficult to see in the EEF filtered in the alpha (7-12 Hz) band. For
762 reference, see Fig. 4 for NMC subjects and Fig. 6 for NVP subjects. The visual evoked potential
763 peaks, i.e., P1, N1, and P2, during the stimulus period (0-240 ms) are related to the perception
764 cycle when the subject looks at an object on the computer screen. The latency of these peaks, i.e.,
765 the delay between the start of the stimulus (0.0 s) and brain response, is very similar for the NMC
766 and NVP subjects. For NMC subjects, these peaks are located at 122 ms, 190 ms, and 305 ms,
767 respectively. For NVP subjects, these peaks are located at 115 ms, 214 ms, and 303 ms,
768 respectively. Remarkably, these peaks for the two groups of subjects are very close to each other.
769 Here, one group consists of eight NMC subjects, and the other consists of eight NVP subjects.
770
771 ----------
772 **Fig. 11. Visual evoked potentials and phase slip rates.** EEG potentials in the broad (3-
773 49 Hz) band and corresponding phase slip rates in the alpha (7-12 Hz) at one of
774 the electrodes in the right visual cortex. (Top) EEG potentials with prominent P1,

N1, and P2 peaks marked, (middle) corresponding PSR1, and (bottom) corresponding PSR2. Notice the subtle differences in EEG peaks and remarkable differences in PSR1 and PSR2 between NMC and NVP subjects.

During the poststimulus period (0.24 - 2.0 s), there are also prominent peaks in the EEG related to brain responses while the subject is analyzing and recognizing the name and form of the object [1]. These perception and decision-making processes extend from 0.0 s to about 1.2 s during the stimulus and poststimulus periods. After that, between 1.2 s and 2.0 s, brain activity begins to return to the regular background activity. Here, the background activity is related to a checkerboard pattern, which is displayed during the prestimulus and poststimulus periods. There are several peaks in the EEG during the poststimulus period of 0.0 to 1.2 s, which are at slightly different locations for NMC and NVP subjects, signifying that brain processes are slightly different for the two groups of subjects during the object recognition process.

The differences between the two groups of subjects are more pronounced when one looks at the temporal patterns of phase slip rates, viz., PSR1 and PSR2, given in the middle and the bottom plots of Fig. 11. The PSR1 is higher for NVP subjects as compared with NMC subjects, while PSR2 has the opposite trend. The PSR2 represents the net rate of number of neurons taking part in the genesis of EEG which one measures at the scalp or subdural electrodes. This suggests that the brain processes of the NMC subjects are changing more rapidly than those of the NVP

subjects. One could probably say that the brain processes are more stable and gradually changing for NVP subjects as compared with NMC subjects.

As stated earlier, the visual evoked potentials, P1, N1, and P2, play a prominent role in the brain's initial response to the object on the screen. Therefore, their spatial analysis is essential and is given in Fig. 12. There are noticeable differences in the spatial profiles of EEG for NMC and NVP subjects. The EEG potentials of P1 for NMC subjects show strong activity in a large area in the lower half of the plot, primarily in the visual, parietal, central, and left temporal regions. In comparison, for NVP subjects, it is mostly concentrated in visual, parietal, and central areas with a slight tilt toward the right side. The N1 positive potential activity for NMC subjects is distributed mainly in the left front and central areas, while for the NVP subjects, it is the left and right top portions of the plots. The negative components for both groups of subjects are distributed in the lower central and right areas. For NMC subjects, it is more focused, while for NVP subjects, it is distributed in larger areas in the lower right area of the plots. For the P2 potentials, both groups show some activity near the nose in the plots, which refers to the brain activity measured at electrodes on the forehead related to cortical activity in the frontal and orbital brain areas. The stark differences are evident in the lower posterior areas, where the NMC subjects exhibit less activity, while the NVP subjects show strong and distributed activity. There is a bright spot in the left frontal area for both groups of subjects.

Fig. 12. **Spatial profiles of P1, N1, and P2 peaks.** Spatial profiles of EEG, PSR1, and PSR2 for visual evoked response potentials, P1, N1, and P2 for NMC and NVP subjects. (Top row) EEG potentials in the broad (3-49 Hz), (middle row) PSR1, and (bottom row) PSR2. The PSR1 and PSR2 are in the alpha (7-12 Hz) band.

The spatial patterns for PSR1 (Fig. 12, middle row) are remarkably different from those of EEG potentials for all three peaks. For the P1 peak of NMC subjects, there is a bright spot near the right ear related to right temporal and auditory cortical brain activity. In contrast, for NVP subjects, there is a bright spot above the left ear, referring to the electrical activity of the left temporal and auditory cortices. Another noticeable difference in PSR1 plots is that NMC subjects have bright spots in the right frontal and central areas, which are missing for NVP subjects. This would suggest that there are some differences in the cortical activity of P1 peaks between NMC and NVP subjects. The PSR1 activity of the N1 peak is also different between NMC and NVP subjects. For the NMC subjects, it has bright spots near the right ear, right frontal, and left posterior central areas. In contrast, for the NVP subjects, PSR1 activity is distributed in the posterior region, near the right ear, and also exhibits some focused bright spots in the left central and parietal midline areas. There are also noticeable differences in the PSR1 plots of P2 peaks for NMC and NVP subjects. A noticeable difference is seen in the right front temporal and central posterior areas. The spatial plots of PSR2 have bright spots, which are well correlated with the bright spots in the PSR1 plots for all three peaks.

The *RDM** and *MAG* values were computed for a comparative analysis between NMC and NVP subjects for all three peaks. These are listed in Table 2. Here, the reference model is the NMC subjects, and the test model is the NVP subjects. As stated earlier, if the reference and test models are the same, then *RDM** will be zero and the *MAG* will be unity. From the values given in the table, it can be inferred that the EEG, PSR1, and PSR2 are significantly different for the NMC and NVP subjects across all three peaks.

Table 2. The *RDM** and *MAG* values for NMC and NVP subjects at the P1, N1, and P2 peaks.

	P1 Peak		N1 Peak		P2 Peak	
	*RDM**	*MAG*	*RDM**	*MAG*	*RDM**	*MAG*
EEG	0.486	1.585	0.976	0.866	0.673	2.290
PSR1	0.849	0.943	0.656	1.430	0.687	1.025
PSR2	0.768	0.880	0.705	0.985	0.635	0.869

D.5 Time Frames of Insight Moments for NMC and NVP Subjects

There are several stages involved in recognizing the name and form of an object from memory [1], and our results indicate that there are subtle timing differences in these stages for NMC and NVP subjects. This is what we are investigating in here. These different stages of insight moments have been described in the literature [1, 36, 49, 43]. Stage I is the first impression of the object in the visual cortex, and it is called the "Awe" moment in the knowledge cycle. It is generally identified with the P1 wave of the visual evoked potentials. Stage II is related to the rapid exploration of the nature of the object in language and memory areas of the brain. The

867 Stage III is the "Eureka" moment when one recognizes and identifies the object. The Stage IV is
868 called the "Verification" stage [1] and it is related to the integration of the new knowledge in the
869 memory for immediate future use, such as in visual object naming tasks. Stage V is the start of
870 the return to the background activity of the brain. These different stages for a frontocentral
871 electrode potentials are marked in Fig. 13A. The EEG potentials are in the 3-49 Hz band. Some
872 of the prominent peaks are also marked, which are also shown in Fig. 3A and Fig. 11.
873
874 --------
875 **Fig. 13.** **Insight moment stages in visual object recognition.** (A) EEG potentials in the
876 3-49 Hz band for one of the electrodes in the frontocentral areas and the
877 associated phase slip rates, PSR1. Different stages of the insight moments are also
878 marked for NMC and NVP subjects. (B) Spatial plots of EEG and PSR1 of the
879 prominent peaks for NMC and NVP subjects, and note their differences.
880 ---------
881
882 The initial first three stages of insight moments are similar, with only minor differences of a few
883 milliseconds for NMC and NVP subjects. However, the duration of the fourth (IV) and fifth (V)
884 stages is different. Stage I is from 0.0 s to the location of the P1 visual evoked potential. This will
885 be the first impression of the object in the visual cortex. The endpoint of stage II is where the P2
886 peak ends, which can be well recognized in the visual evoked potentials given in Figs. 2 and 10.
887 Stage III (305–561 ms) is the “Eureka” moment, when one recognizes and identifies the object
888 [1, 36].

889 Stage IV is related to integrating the new knowledge into memory [1]. The Stage IV for the NVP
890 subjects is from 561 to 702 ms, i.e., with a duration of 141 ms. In contrast, the Stage IV duration
891 for NMC subjects is longer, ranging from 561 ms to 831 ms, with a total duration of 270 ms.
892 Stages III and IV are critical stages in the process of identifying and assimilating new knowledge
893 into memory. NVP subjects seem to be quicker at assimilating new knowledge into memory than
894 NMC subjects. This is also reflected in the bimodal shape of the PSR1 activity for NVP subjects
895 (lower plot in Fig. 13A). *So, for NVP subjects, it takes 702 ms from the start of the stimulus to*
896 *identify and assimilate the new knowledge into memory. In comparison, for the same task, it took*
897 *831 ms for NMC subjects.* Stage V marks the beginning of a return to background brain activity
898 [1, 43].
899
900 The additional prominent peaks during the knowledge cycle, identified in Fig. 13A, are N707,
901 P787, and N905. The spatial plots of EEG (3-49 Hz) potentials and their respective PSR1 are
902 given in Fig. 13 B. The spatial plots of the EEG potentials for NMC and NVP subjects are
903 significantly different ($p < 0.01$), which was confirmed by the paired Student's t-test. Spatial
904 differences are also noticeable for these three peaks between NMC and NVP subjects. For the
905 N707 peak, the RDM* and MAG between NMC and NVP subjects were: 0.697 and 1.19. The
906 same comparative values for the peak P787 were: 0.787 and 1.03. For the peak N905, these were:
907 0.85 and 1.29. These values suggest that the spatial plots of PSR1 for the NMC and NVP
908 subjects are significantly different from each other.
909
910 **E. Discussions**

911 Our primary objective was to quantify the differences in decision-making processes between
912 NMC and NVP subjects. Our results demonstrate quantifiable differences in four biomarkers that
913 we utilized in this study. The temporal and spatial patterns of EEG, EEG′, PSR1, and PSR2
914 indicate that different brain regions are activated in NMC and NVP subjects. Another remarkable
915 finding is that NVP subjects are quicker (702 ms) compared to NMC subjects (831 ms) in
916 completing the visual task of identifying and assimilating new knowledge into memory. This is a
917 remarkable finding that suggests people can be trained to perform tasks more efficiently for
918 visual object recognition. The emphasis here is on visual object recognition processes, which are
919 commonly employed in various meditation techniques. This finding not only suggests potential
920 applications in other meditative techniques but also underscores the need for further research in
921 this field. It also suggests that similar results may be observed in other tasks, such as motor
922 function-related tasks, which should be examined through carefully designed studies comparing
923 non-meditator control subjects with those who have undergone meditative training in those
924 particular tasks. An example of motor function-related tasks is the use of hand gestures, i.e.,
925 Mudras, which are very common in meditation practices.
926
927 Although many studies have been conducted to examine the efficacy of Vipassana in the context
928 of mindfulness-based interventions, relatively few studies have focused on traditional Vipassana
929 practitioners. Prior work from our group has examined EEG profiles of three proficiency-linked
930 groups of Vipassana meditation practitioners while they engaged in a structured sequence of
931 meditation practice (Anapana or focused attention, Vipassana or mindfulness, and Metta or
932 loving-kindness) and found that long-term meditators (seniors and teachers) showed widespread

933 trait and state differences as compared to novice meditators [28]. Examination of P300 dynamics
934 in the same three groups of meditators during the performance of the ANGEL task had revealed
935 significant state-trait influences of meditation practice [29]. Future work could therefore evaluate
936 the applicability of the four biomarkers employed in the current study across distinct meditation
937 states in NVPs and in long-term meditators.
938
939 Our work with novice Vipassana-trained subjects was facilitated by the availability of their data
940 sets and can be readily applied to other datasets from Vipassana meditators [50]. However, the
941 techniques and tools developed for this work are generic and versatile, and can be potentially
942 applied to any EEG data set to augment the existing set of measures. For instance, these tools can
943 be used to study the behavior of default mode networks in the spontaneous EEG or evoked
944 potential studies [51]. Similarly, our tools are applicable across diverse meditation practices,
945 including Zen, Mindfulness, Insight, other Buddhist and non-Buddhist traditions [52, 53, 54, 55].
946 Indeed, recent work examining EEG data from four different meditation traditions revealed both
947 a common core and tradition-specificity in the neurodynamic profiles [56]. When the mind is
948 trained to remain stable and focused, tools from our current work can augment traditional
949 measures in detecting subtle changes in brain activity from EEG data [57, 58]. Their sensitivity
950 extends to calm-abiding practices that cultivate stability and insight (Samatha & Vipassana) and
951 to practices that foster compassion, generosity, morality, joyous effort, and loving-kindness [59,
952 60, 61]. We hope that other investigators will adopt these tools in their research work.
953

We have used four biomarkers in this study. The spatial profiles of EEG and EEG′ are similar, with some minor differences which are not significant. Similarly, the spatial differences in the PSR1 and PSR2 plots are also minor. However, there are some significant differences between the spatial plots of EEG and its related PSR1, as well as between EEG′ and PSR2, that require explanation. Refer to Figs. 6 and 8. We first introduced these biomarkers in our recent work [4], where we mentioned that the first-order derivative of the EEG data removes linear trends and amplifies nonlinear trends and oscillatory activity in the data. The computation of the phase from EEG or EEG′ by use of the Hilbert transform does not depend upon the amplitude of the data but rather on large and small perturbations in the data. Even at the small perturbations in the data, a $\pm\pi$ phase shift is introduced, which could influence the computations of PSR1 and PSR2 at numerous spatial locations. Additionally, within a given time slice of the EEG (or EEG′) data, large amplitude values may occur on a few channels, while small perturbations in the data may occur on other channels. Thus, the spatial locations of PSR1 and PSR2 could be different from the spatial locations of EEG or EEG′, respectively. These could be the reasons why the EEG and PSR1, as well as EEG′ and PSR2, show some significant differences in the spatial plots. One could verify these by source location analysis from EEG and PSR1, or from EEG' and PSR2. This is a significantly big task, perhaps suitable for a separate study.

Our results, in line with earlier research [4], underscore the robustness of phase slip activity across broader brain areas, even when EEG potentials are low or near the zero-crossing lines. This robustness suggests that phase slip rates could be a more sensitive biomarker than EEG or EEG′ for detecting changes in brain activity. Importantly, this could significantly enhance our

976 understanding of brain functions, particularly in scenarios such as the study of the EEG of
977 anesthetized patients [62], the EEG data of subjects engaged in the Tukdum practice of Buddhist
978 meditation near the time of death [63], or the EEG of subjects going through near-death
979 experiences [64]. In these situations, the use of phase slip rate biomarkers derived from EEG, as
980 well as the first and second-order derivatives of EEG, could provide valuable insights into brain
981 activity, where EEG alone may not be sensitive enough to detect widespread changes in brain
982 activity [4]. Furthermore, phase slip rates could serve as a sensitive gauge to monitor the level of
983 anesthesia or the patient's level of consciousness during surgery or meditation.
984
985 Here, we have limited our work to the alpha (7-12 Hz) band only, which, in general, is the most
986 predominant band in the power spectrum and also plays a crucial role in visual object recognition
987 and insight moment analysis studies [1]. In future studies, this work could be extended to other
988 EEG bands, such as theta, alpha, beta, and gamma bands, which may provide additional insights
989 into the similarities and differences between NMC and NVP subjects in decision making
990 processes. Additionally, phase amplitude couplings between different bands, such as theta-alpha
991 or beta-gamma bands, may be another area to explore.
992
993 In summary, we demonstrated that cortical phase transitions alter during decision making and
994 that brain functions differ between non-meditators and novice Vipassana meditators. These
995 methods and results may aid future experimental designs in visual cognition and mindfulness
996 research, as well as contribute to educational neuroscience and the development of
997 neurofeedback technologies for clinical applications. This is our hope.

F. Data availability statement

Publicly available data sets were used in this study. This data can be found at: https://osf.io.

G. Author contributions

RJK: Conceptualization, Methodology, Writing – original draft, Writing – review & editing.

AKN: Data curation, Data analysis, Writing – original draft, Writing – review & editing.

AS: Data curation, Data analysis, Writing – review & editing.

RV: Data Curation.

PNR: Project administration, Supervision, Writing – review & editing.

BK: Project administration, Supervision, Writing – review & editing.

CR: Conceptualization, Methodology, Data curation, Data analysis, Software, Visualization, Writing – original draft, Writing – review & editing.

H. Funding

No funding for this project

I. Conflict of interest

The authors declare that the research was conducted in the absence of any commercial or financial relationships that could be construed as a potential conflict of interest.

J. Acknowledgment

Professor Jens Hauesien from the Technical University of Ilmenau, Germany, made several technical and grammatical suggestions to improve the manuscript's writing. We want to thank him for his efforts.

1027 **Figure Captions**

1028

1029 **Fig. 1. Vipassana Meditation.**

1030 Schematic representation of the Vipassana practice in the tradition of Sayagyi U Ba Khin

1031 as taught by S.N. Goenka.

1032

1033 **Fig. 2. Audiovisual oddball task.**

1034 Protocol Diagram from earlier publication. Representative examples from two types of

1035 task blocks. (From Nair et al., 2016).

1036

1037 **Fig. 3. EEG traces and spatial profiles.**

1038 An example of an EEG trace after preprocessing for two electrodes in a 3-49 Hz

1039 broadband. (A) EEG from one of the electrodes in the frontocentral area, (B) EEG from

1040 one of the electrodes in the right visual area, and (C) spatial profile of EEG potentials at

1041 the P1 peak of the NVP subject. Note that the time series profiles of PSRs at two

1042 electrodes are significantly different during the 0.0-1.0 s period, when the subject is

1043 visualizing and analyzing the image of the object during covert object naming tasks.

1044

1045 **Fig. 4. A pictorial representation of the phase slip extraction steps.**

1046 Plots in the left column are marked in (A) for the phase slips extraction from the EEG,

1047 and, similarly, the right column (B) is for the phase slips extraction from EEG′, i.e., from

1048 the first order derivative of EEG. The top row is the EEG and EEG′, the second row from

the top is the sawtooth pattern of the phase, the third row from the top is the unwrapped phase, and the bottom row shows some of the phase slips.

Fig. 5. EEG, its derivative, and phase slip rates.

Temporal plots of quantities of one of the electrodes in the front central area for non-meditator control (NMC) subjects. (Top left) EEG in 3-49 Hz band, (top right) EEG′ in 3-49 Hz band, (middle left) EEG filtered in the alpha band of 7-12 Hz, (middle right) EEG′ filtered in the alpha band of 7-12 Hz, (bottom left) phase slip rate PSR1 extracted from EEG in the alpha band, and (bottom right) phase slip rate PSR2 extracted from EEG′ in the alpha band. Notice the prominent peaks in PSR1 and PSR2 related to brain activity during the visual object recognition tasks. The prestimulus period is from -1.0 to 0.0 s. The combined stimulus and poststimulus period, referred to as the poststimulus+ period, spans from 0.0 to 2.0 seconds.

Fig. 6. Plots of EEG and PSR of non-meditator control (NMC) subjects.

Spatiotemporal plots of the root mean square (RMS) values of EEG and its first order derivative (EEG′) and their associated mean values of phase slip rates for non-meditator control (NMC) subjects. The RMS and mean values were computed within a 0.5 s stepping window. The temporal duration for each frame is given at the top. (A) The top two rows are for the RMS EEG and the mean PSR1, respectively. (B) The bottom two rows are for the RMS EEG′ and the mean PSR2. Notice the shifting spatial patterns of all four quantities.

1071 **Fig. 7. One electrode plot of NVP subjects.**

1072 Temporal plots of quantities of one of the electrodes in the front central area for novice
1073 Vipassana (NVP) subjects. (Top left) EEG in 3-49 Hz band, (top right) EEG′ in 3-49 Hz
1074 band, (middle left) EEG filtered in the alpha band of 7-12 Hz, (middle right) EEG′
1075 filtered in the alpha band of 7-12 Hz, (bottom left) phase slip rate PSR1 extracted from
1076 EEG in the alpha band, and (bottom right) phase slip rate PSR2 extracted from EEG′ in
1077 the alpha band. Notice the prominent peaks in PSR1 and PSR2 related to brain activity
1078 during the visual object recognition tasks.

1079

1080 **Fig. 8. Plots of EEG, its derivative, and PSR of NVP subjects.**

1081 Spatiotemporal plots of the root mean square (RMS) values of EEG and EEG′ and their
1082 associated mean values of phase slip rates for novice Vipassana (NVP) subjects. The
1083 RMS and mean values were computed in the stepping window of 0.5 s duration. The
1084 temporal duration for each frame is given at the top. (A) The top two rows are for the
1085 RMS EEG and the mean PSR1, and (B) the bottom two rows are for the RMS EEG′ and
1086 the mean PSR2, respectively. Notice the shifting spatial patterns of all four quantities
1087 from Frame 1 to Frame 6.

1088

1089 **Fig. 9. Activity patterns of EEG and PSR1 above baseline.**

1090 (A) Spatial plots of RMS EEG above the baseline of NMC and NVP subjects, (B)
1091 corresponding spatial plots of mean PSR1 above the baseline, (C) histogram distribution

of RMS EEG values shown in spatial plots of A, and (D) histogram distribution of PSR1values shown in spatial plots of B.

Fig. 10. **Activity patterns of the first derivative of EEG and PSR2 above baseline.**

(A) Spatial plots of RMS EEG′ above the baseline of NMC and NVP subjects, (B) corresponding spatial plots of mean PSR2 above the baseline, (C) histogram distribution of the RMS EEG′ values shown in spatial plots of A, and (D) histogram distribution of PSR2 values shown in spatial plots of B.

Fig. 11. **Visual evoked potentials and phase slip rates.**

EEG potentials in the broad (3-49 Hz) band and corresponding phase slip rates in the alpha (7-12 Hz) at one of the electrodes in the right visual cortex. (Top) EEG potentials with prominent P1, N1, and P2 peaks marked, (middle) corresponding PSR1, and (bottom) corresponding PSR2. Notice the subtle differences in EEG peaks and remarkable differences in PSR1 and PSR2 between NMC and NVP subjects.

Fig. 12. **Spatial profiles of P1, N1, and P2 peaks.**

Spatial profiles of EEG, PSR1, and PSR2 for visual evoked response potentials, P1, N1, and P2 for NMC and NVP subjects. (Top row) EEG potentials in the broad (3-49 Hz) band, (middle row) PSR1, and (bottom row) PSR2. The PSR1 and PSR2 are in the alpha (7-12 Hz) band.

Fig. 13. Insight moment stages in visual object recognition.

(A) EEG potentials in the 3-49 Hz band for one of the electrodes in the frontocentral areas and the associated phase slip rates, PSR1. Different stages of the insight moments are also marked for NMC and NVP subjects. (B) Spatial plots of EEG and PSR1 of the prominent peaks for NMC and NVP subjects, and note their differences.

1121 **References**

1122

1123 1. Ramon C, Graichen U, Gargiulo P, Zanow F, Knösche TR, Haueisen J. Spatiotemporal
1124 phase slip patterns for visual evoked potentials, covert object naming tasks, and insight
1125 moments extracted from 256 channel EEG recordings. Front Integr Neurosci. 2023 Jun
1126 13;17: 1087976. doi: 10.3389/fnint.2023.1087976.

1127 2. Ramon C, Doud A, Holmes MD. Decrease in phase slip rates and phase cone structures
1128 during seizure evolution and epileptogenic activities derived from microgrid ECoG data.
1129 Curr Res Neurobiol. 2024 Feb 19;6: 100126. doi: 10.1016/j.crneur.2024.100126.

1130 3. Freeman WJ, Holmes MD, West GA, Vanhatalo S. Fine spatiotemporal structure of
1131 phase in human intracranial EEG. Clin Neurophysiol. 2006 Jun;117(6): 1228-43. doi:
1132 10.1016/j.clinph.2006.03.012.

1133 4. Ramon C, Gargiulo P. Phase slips extracted from derivatives of EEG data provide a
1134 deeper insight into the formation of cortical phase transitions. Front Integr Neurosci. 2025
1135 Feb 25;19: 1471120. doi: 10.3389/fnint.2025.1471120.

1136 5. Woodman GF. A brief introduction to the use of event-related potentials in studies of
1137 perception and attention. Atten Percept Psychophys. 2010 Nov;72(8): 2031-46. doi:
1138 10.3758/APP.72.8.2031.

1139 6. Kounios J, Fleck JI, Green DL, Payne L, Stevenson JL, Bowden EM, Jung-Beeman M.
1140 The origins of insight in resting-state brain activity. Neuropsychologia. 2008 Jan
1141 15;46(1): 281-91. doi: 10.1016/j.neuropsychologia.2007.07.013. Epub 2007 Jul 27.

7. Cocchi L, Gollo LL, Zalesky A, Breakspear M. Criticality in the brain: A synthesis of neurobiology, models and cognition. Prog Neurobiol. 2017 Nov;158: 132-152. doi: 10.1016/j.pneurobio.2017.07.002. Epub 2017 Jul 19.

8. Heffern EFW, Huelskamp H, Bahar S, Inglis RF. Phase transitions in biology: from bird flocks to population dynamics. Proc Biol Sci. 2021 Oct 27;288(1961): 20211111. doi: 10.1098/rspb.2021.1111. Epub 2021 Oct 20

9. Wang SH, Siebenhühner F, Arnulfo G, Myrov V, Nobili L, Breakspear M, Palva S, Palva JM. Critical-like Brain Dynamics in a Continuum from Second- to First-Order Phase Transition. J Neurosci. 2023 Nov 8;43(45): 7642-7656. doi: 10.1523/JNEUROSCI.1889-22.2023. Epub 2023 Oct 10.

10. Bak P, Tang C, Wiesenfeld K. Self-organized criticality: An explanation of the 1/f noise. Phys Rev Lett. 1987 Jul 27;59(4): 381-384. doi: 10.1103/PhysRevLett.59.381.

11. Dhar D. Self-organized critical state of sandpile automaton models. Phys Rev Lett. 1990 Apr 2;64(14): 1613-1616. doi: 10.1103/PhysRevLett.64.1613.

12. Holt AB, Kormann E, Gulberti A, Pötter-Nerger M, McNamara CG, Cagnan H, Baaske MK, Little S, Köppen JA, Buhmann C, Westphal M, Gerloff C, Engel AK, Brown P, Hamel W, Moll CKE, Sharott A. Phase-Dependent Suppression of Beta Oscillations in Parkinson's Disease Patients. J Neurosci. 2019 Feb 6;39(6): 1119-1134. doi: 10.1523/JNEUROSCI.1913-18.2018. Epub 2018 Dec 14.

13. di Santo S, Villegas P, Burioni R, Muñoz MA. Landau-Ginzburg theory of cortex dynamics: Scale-free avalanches emerge at the edge of synchronization. Proc Natl Acad

1163 Sci U S A. 2018 Feb 13;115(7): E1356-E1365. doi: 10.1073/pnas.1712989115. Epub
1164 2018 Jan 29.
1165 14. Tognoli E, Kelso JA. The metastable brain. Neuron. 2014 Jan 8;81(1): 35-48. doi:
1166 10.1016/j.neuron.2013.12.022.
1167 15. Kozma R, Freeman WJ. Cinematic Operation of the Cerebral Cortex Interpreted via
1168 Critical Transitions in Self-Organized Dynamic Systems. Front Syst Neurosci. 2017 Mar
1169 14;11: 10. doi: 10.3389/fnsys.2017.00010.
1170 16. Beggs JM, Timme N. Being critical of criticality in the brain. Front Physiol. 2012 Jun
1171 7;3: 163. doi: 10.3389/fphys.2012.00163.
1172 17. Freeman WJ, Vitiello G. Nonlinear brain dynamics as macroscopic manifestation of
1173 underlying many-body field dynamics. Phys. Life Rev. 2006; 3(2): 93–118. doi:
1174 10.1016/j.plrev.2006.02.001.
1175 18. Freeman WJ, Vitiello G. Vortices in brain waves. International Journal of Modern
1176 Physics B. 2010 Jul 10;24(17): 3269-95. doi: 10.1142/S0217979210056025.
1177 19. Ramon C, Holmes MD, Wise MV, Tucker D, Jenson K, Kinn SR. Oscillatory Patterns of
1178 Phase Cone Formations near to Epileptic Spikes Derived from 256-Channel Scalp EEG
1179 Data. Comput Math Methods Med. 2018 Nov 21;2018: 9034543. doi:
1180 10.1155/2018/9034543.
1181 20. Grossman, P. Mindfulness for Psychologists: Paying Kind Attention to the Perceptible.
1182 Mindfulness. 2010; 1: 87–97. doi: 10.1007/s12671-010-0012-7.

1183 21. Bishop SR, Lau M, Shapiro S, Carlson L, Anderson ND, Carmody J, Segal ZV, Abbey S,
1184 Speca M, Velting D, Devins G. Mindfulness: A Proposed Operational Definition. Clinical
1185 Psychology: Science and Practice. 2004; 11: 230-241. doi: 10.1093/clipsy.bph077.
1186 22. Walsh R. Meditation. In: Corsini RJ, editor. Handbook of innovative psychotherapy. New
1187 York: John Wiley & Sons Inc.; 2001. pp. 368-380.
1188 23. Attrey S, Joshi S, Bhatt V. Mindful path to psychological wellbeing: a comprehensive
1189 review. Journal of Behavioral and Cognitive Therapy. 2025; 35(4), 100537. doi:
1190 10.1016/j.jbct.2025.100537.
1191 24. Siegel DJ. Mindfulness training and neural integration: differentiation of distinct streams
1192 of awareness and the cultivation of well-being. Soc Cogn Affect Neurosci. 2007
1193 Dec;2(4): 259–63. doi: 10.1093/scan/nsm034.://doi.org/10.1093/scan/nsm034.
1194 25. Tang YY, Hölzel BK, Posner MI. The neuroscience of mindfulness meditation. Nat Rev
1195 Neurosci. 2015 Apr;16(4): 213-25. doi: 10.1038/nrn3916. Epub 2015 Mar 18.
1196 26. Awasthi B. Issues and perspectives in meditation research: in search for a definition.
1197 Front Psychol. 2013 Jan 10;3: 613. doi: 10.3389/fpsyg.2012.00613.
1198 27. Ivanovski B, Malhi GS. The psychological and neurophysiological concomitants of
1199 mindfulness forms of meditation. Acta Neuropsychiatr. 2007 Apr;19(2): 76-91. doi:
1200 10.1111/j.1601-5215.2007.00175.x.
1201 28. Kakumanu RJ, Nair AK, Venugopal R, Sasidharan A, Ghosh PK, John JP, Mehrotra S,
1202 Panth R, Kutty BM. Dissociating meditation proficiency and experience dependent EEG
1203 changes during traditional Vipassana meditation practice. Biol Psychol. 2018 May;135:
1204 65-75. doi: 10.1016/j.biopsycho.2018.03.004. Epub 2018

1205 29. Kakumanu RJ, Nair AK, Sasidharan A, John JP, Mehrotra S, Panth R, Kutty BM.
1206 State-trait influences of Vipassana meditation practice on P3 EEG dynamics. Prog Brain
1207 Res. 2019;244: 115-136. doi: 10.1016/bs.pbr.2018.10.027. Epub 2019 Jan 22.
1208 30. Goenka SN. The Discourse Summaries. Igatpuri, India: Vipassana Research Institute;
1209 1987.
1210 31. Goenka, S. N. (1991). Buddha's Path is to Experience Reality. Sayagyi U Ba Khin
1211 Journal. 1991; 109: 13.
1212 32. U Ba Khin S. The Essentials of Buddha-Dhamma in Meditative Practice. In: Sayagyi U
1213 Ba Khin. Onalaska, WA, USA: Vipassana Research Publications, Pariyatti Publishing;
1214 1991. pp. 12-22.
1215 33. Ñanamoli T. The Practice of Loving-Kindness (Metta): As Taught by the Buddha in the
1216 Pali Canon. In The Four Sublime States Contemplations on Love, Compassion,
1217 Sympathetic Joy, and Equanimity (BPS online). Kandy, Sri Lanka: Buddhist Publication
1218 Society. 1994; Retrieved on 25 August 2025,
1219 http://www.accesstoinsight.org/lib/authors/nanamoli/wheel007.html
1220 34. Wallas G. The Art of Thought. New York: Harcourt, Brace and Company; 1926. pp. 10.
1221 35. Gell-Mann M. The Quark and the Jaguar: Adventures in the Simple and the Complex.
1222 New York: W.H. Freeman; 1994. pp. 264–265.
1223 36. Sadler-Smith E. Wallas' Four-Stage model of the creative process: more than meets the
1224 eye?. Creativity Research Journal. 2015; 27(4): 342-352. doi:
1225 10.1080/10400419.2015.1087277.

1226 37. Kounios J, Beeman M. The cognitive neuroscience of insight. Annu Rev Psychol.
1227 2014;65: 71-93. doi: 10.1146/annurev-psych-010213-115154.
1228 38. Oh Y, Chesebrough C, Erickson B, Zhang F, Kounios J. An insight-related neural reward
1229 signal. Neuroimage. 2020 Jul 1;214: 116757. doi: 10.1016/j.neuroimage.2020.116757.
1230 Epub 2020 Mar 16.
1231 39. Salvi C, Bricolo E, Franconeri SL, Kounios J, Beeman M. Sudden insight is associated
1232 with shutting out visual inputs. Psychon Bull Rev. 2015 Dec;22(6): 1814-9. doi:
1233 10.3758/s13423-015-0845-0.
1234 40. Nair AK, Sasidharan A, John JP, Mehrotra S, Kutty BM. Assessing Neurocognition via
1235 Gamified Experimental Logic: A Novel Approach to Simultaneous Acquisition of
1236 Multiple ERPs. Front Neurosci. 2016 Jan 29;10: 1. doi: 10.3389/fnins.2016.00001.
1237 41. Delorme A, Makeig S. EEGLAB: an open source toolbox for analysis of single-trial EEG
1238 dynamics including independent component analysis. J Neurosci Methods. 2004 Mar
1239 15;134(1): 9-21. doi: 10.1016/j.jneumeth.2003.10.009.
1240 42. Davis JJ, Kozma R, Freeman WJ. Neurophysiological evidence of the cognitive cycle and
1241 the emergence of awareness. In: 2013 International Joint Conference on Awareness
1242 Science and Technology & Ubi-Media Computing (iCAST 2013 & UMEDIA 2013) 2013
1243 Nov 2 (pp. 149-157). IEEE. doi.: 10.1109/ICAwST.2013.6765425.
1244 43. Myers MH, Kozma R, Davis JJ, Ilin R. (2014). Phase cone detection optimization in EEG
1245 data. In: Proceedings of the 2014 international joint conference on neural networks
1246 (IJCNN). Piscataway, NJ: IEEE; 2014. pp. 2504–2511. doi:
1247 10.1109/IJCNN.2014.6889880

1248 44. Kobayashi K, Shibata T, Tsuchiya H, Akiyama T. Exclusion of the Possibility of "False
1249 Ripples" From Ripple Band High-Frequency Oscillations Recorded From Scalp
1250 Electroencephalogram in Children With Epilepsy. Front Hum Neurosci. 2021 Jun 15;15:
1251 696882. doi: 10.3389/fnhum.2021.696882.
1252 45. Ramon C, Holmes MD. Stochastic Behavior of Phase Synchronization Index and
1253 Cross-Frequency Couplings in Epileptogenic Zones during Interictal Periods Measured
1254 with Scalp dEEG. Front Neurol. 2013 May 16;4: 57. doi: 10.3389/fneur.2013.00057.
1255 46. Freeman WJ, Rogers LJ. Fine temporal resolution of analytic phase reveals episodic
1256 synchronization by state transitions in gamma EEGs. J Neurophysiol. 2002 Feb;87(2):
1257 937-45. doi: 10.1152/jn.00254.2001.
1258 47. Varela F, Lachaux JP, Rodriguez E, Martinerie J. The brainweb: phase synchronization
1259 and large-scale integration. Nat Rev Neurosci. 2001 Apr;2(4): 229-39. doi:
1260 10.1038/35067550.
1261 48. Lancaster G, Iatsenko D, Pidde A, Ticcinelli V, Stefanovska A. Surrogate data for
1262 hypothesis testing of physical systems. Physics Reports. 2018 Jul 18; 748: 1-60. doi:
1263 10.1016/j.physrep.2018.06.001.
1264 49. Lee JY, Lindquist KA, Nam CS. Emotional Granularity Effects on Event-Related Brain
1265 Potentials during Affective Picture Processing. Front Hum Neurosci. 2017 Mar 24;11:
1266 133. doi: 10.3389/fnhum.2017.00133.
1267 50. Cahn BR, Delorme A, Polich J. Occipital gamma activation during Vipassana meditation.
1268 Cogn Process. 2010 Feb;11(1): 39-56. doi: 10.1007/s10339-009-0352-1. Epub 2009 Dec
1269 16.

1270 51. Berkovich-Ohana A, Glicksohn J, Goldstein A. Studying the default mode and its
1271 mindfulness-induced changes using EEG functional connectivity. Soc Cogn Affect
1272 Neurosci. 2014 Oct;9(10): 1616-24. doi: 10.1093/scan/nst153. Epub 2013 Nov 4.
1273 52. Brefczynski-Lewis JA, Lutz A, Schaefer HS, Levinson DB, Davidson RJ. Neural
1274 correlates of attentional expertise in long-term meditation practitioners. Proc Natl Acad
1275 Sci U S A. 2007 Jul 3;104(27): 11483-8. doi: 10.1073/pnas.0606552104. Epub 2007 Jun
1276 27.
1277 53. Hinterberger T, Schmidt S, Kamei T, Walach H. Decreased electrophysiological activity
1278 represents the conscious state of emptiness in meditation. Front Psychol. 2014 Feb 17;5:
1279 99. doi: 10.3389/fpsyg.2014.00099.
1280 54. Lomas T, Ivtzan I, Fu CH. A systematic review of the neurophysiology of mindfulness on
1281 EEG oscillations. Neurosci Biobehav Rev. 2015 Oct;57: 401-10. doi:
1282 10.1016/j.neubiorev.2015.09.018. Epub 2015 Oct 9.
1283 55. Schoenberg PLA, Ruf A, Churchill J, Brown DP, Brewer JA. Mapping complex mind
1284 states: EEG neural substrates of meditative unified compassionate awareness. Conscious
1285 Cogn. 2018 Jan;57: 41-53. doi: 10.1016/j.concog.2017.11.003. Epub 2017 Nov 21.
1286 56. Shrimali P, Sasidharan A, Malipeddi S, Ventura B, Venugopal R, Nair A K, et al. Similar
1287 States, Different Paths: Neurodynamics of diverse meditation techniques. bioRxiv
1288 2025.06.20.660652 [Preprint] 2025 [cited 2025 August 28]. Available from:
1289 https://doi.org/10.1101/2025.06.20.660652
1290 57. Malipeddi S, Sasidharan A, Pinna Nagendra R, Mehrotra S, P John J, M Kutty B. Data
1291 from "Relaxed alertness in novice and advanced meditators – A neurophysiological and

1292 psychological study of Isha Yoga practices". Mindfullness. Zenodo; 2024 Oct;
1293 https://doi.org/10.5281/zenodo.13969788.
1294 58. Nair AK, Sasidharan A, John JP, Mehrotra S, Kutty BM. Just a minute meditation: Rapid
1295 voluntary conscious state shifts in long term meditators. Conscious Cogn. 2017 Aug;53:
1296 176-184. doi: 10.1016/j.concog.2017.06.002. Epub 2017 Jul 5.
1297 59. Huang C, Kaliman P, Epel ES, Saron CD. Insight meditation and telomere biology: The
1298 effects of intensive retreat and the moderating role of personality. Brain Behav Immun.
1299 2018 May;70: 233-245. doi: 10.1016/j.bbi.2018.03.003. Epub 2018 Mar 5. Erratum in:
1300 Brain Behav Immun. 2018 Oct;73: 736-737. doi: 10.1016/j.bbi.2018.07.015.
1301 60. Nair AK, John JP, Mehrotra S, Kutty BM. What contributes to wellbeing gains –
1302 proficiency or duration of meditation related practices?. International Journal of
1303 Wellbeing. 2018 Dec 8; 8(2). doi: 10.5502/ijw.v8i2.696.
1304 61. Sankar Sylapan B, Nair AK, Jayanna K, Mallipeddi S, Sathyanarayana S, Kutty BM.
1305 Meditation, well-being and cognition in heartfulness meditators - A pilot study.
1306 Conscious Cogn. 2020 Nov;86: 103032. doi: 10.1016/j.concog.2020.103032. Epub 2020
1307 Oct 20.
1308 62. Purdon PL, Sampson A, Pavone KJ, Brown EN. Clinical Electroencephalography for
1309 Anesthesiologists: Part I: Background and Basic Signatures. Anesthesiology. 2015
1310 Oct;123(4): 937-60. doi: 10.1097/ALN.0000000000000841.
1311 63. Lott DT, Yeshi T, Norchung N, Dolma S, Tsering N, Jinpa N, Woser T, Dorjee K, Desel
1312 T, Fitch D, Finley AJ, Goldman R, Bernal AMO, Ragazzi R, Aroor K, Koger J, Francis
1313 A, Perlman DM, Wielgosz J, Bachhuber DRW, Tamdin T, Sadutshang TD, Dunne JD,

1314 Lutz A, Davidson RJ. No Detectable Electroencephalographic Activity After Clinical
1315 Declaration of Death Among Tibetan Buddhist Meditators in Apparent Tukdam, a
1316 Putative Postmortem Meditation State. Front Psychol. 2021 Jan 28;11: 599190. doi:
1317 10.3389/fpsyg.2020.599190.
1318 64. Martial C, Fritz P, Gosseries O, Bonhomme V, Kondziella D, Nelson K, Lejeune N. A
1319 neuroscientific model of near-death experiences. Nat Rev Neurol. 2025 Jun;21(6):
1320 297-311. doi: 10.1038/s41582-025-01072-z. Epub 2025 Mar 31. Erratum in: Nat Rev
1321 Neurol. 2025 Aug;21(8):465. doi: 10.1038/s41582-025-01111-9.
1322
1323

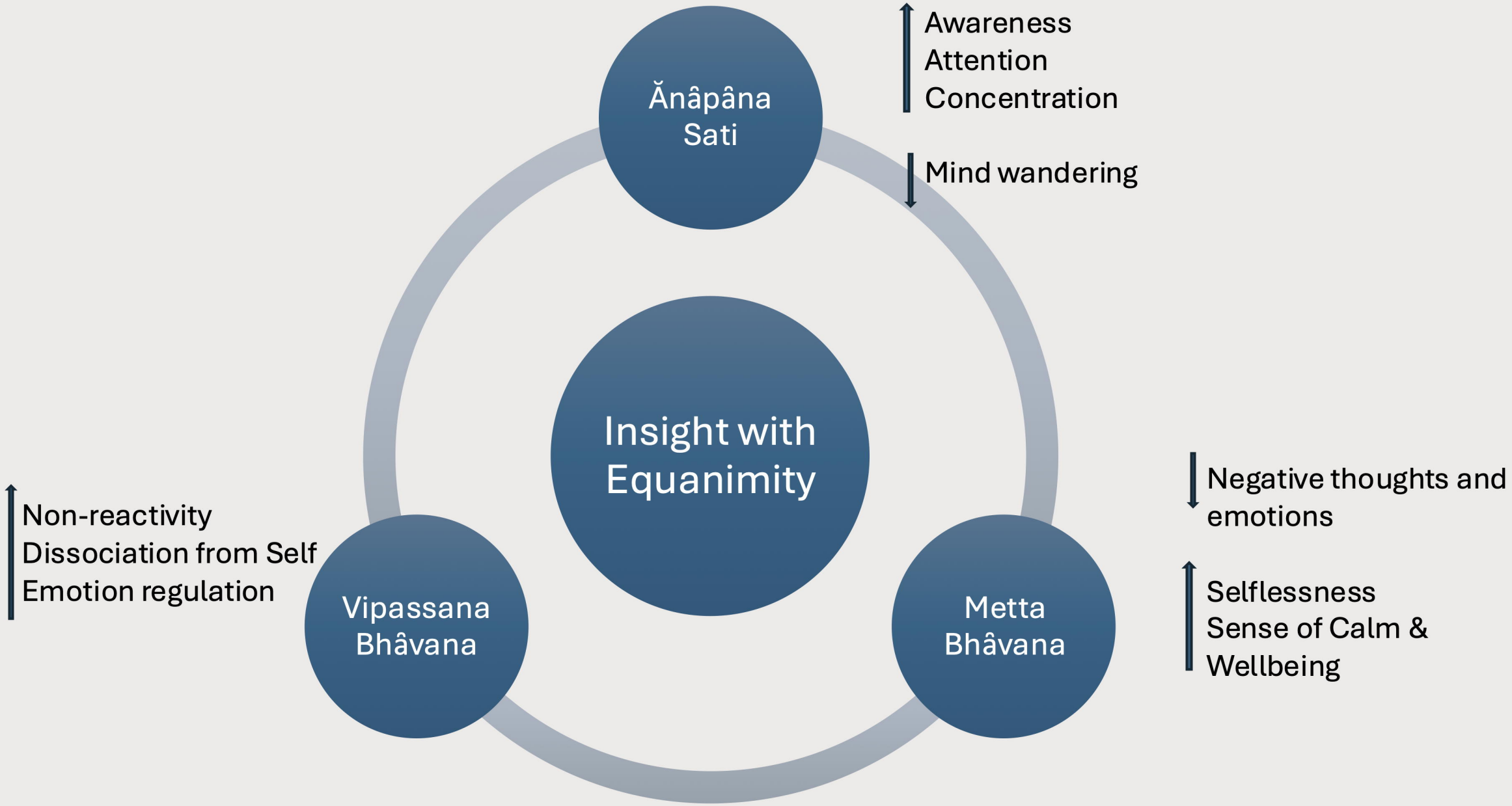
Ănâpâna Sati
Awareness
Attention
Concentration
Mind wandering
Insight with Equanimity
Negative thoughts and emotions
Selflessness
Sense of Calm & Wellbeing
Metta Bhâvana
Vipassana Bhâvana
Non-reactivity
Dissociation from Self
Emotion regulation

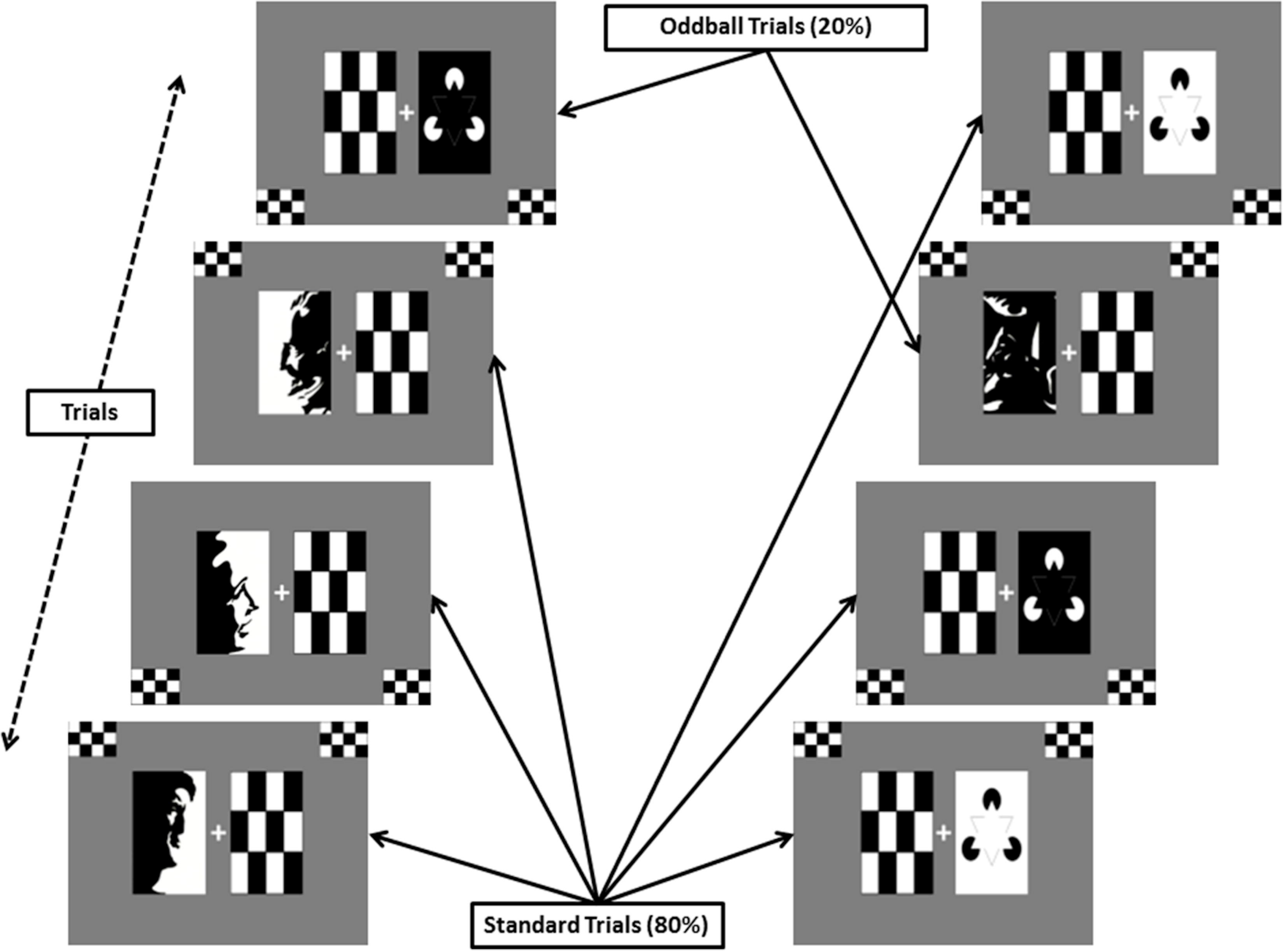
Oddball Trials (20%)
Trials
Standard Trials (80%)

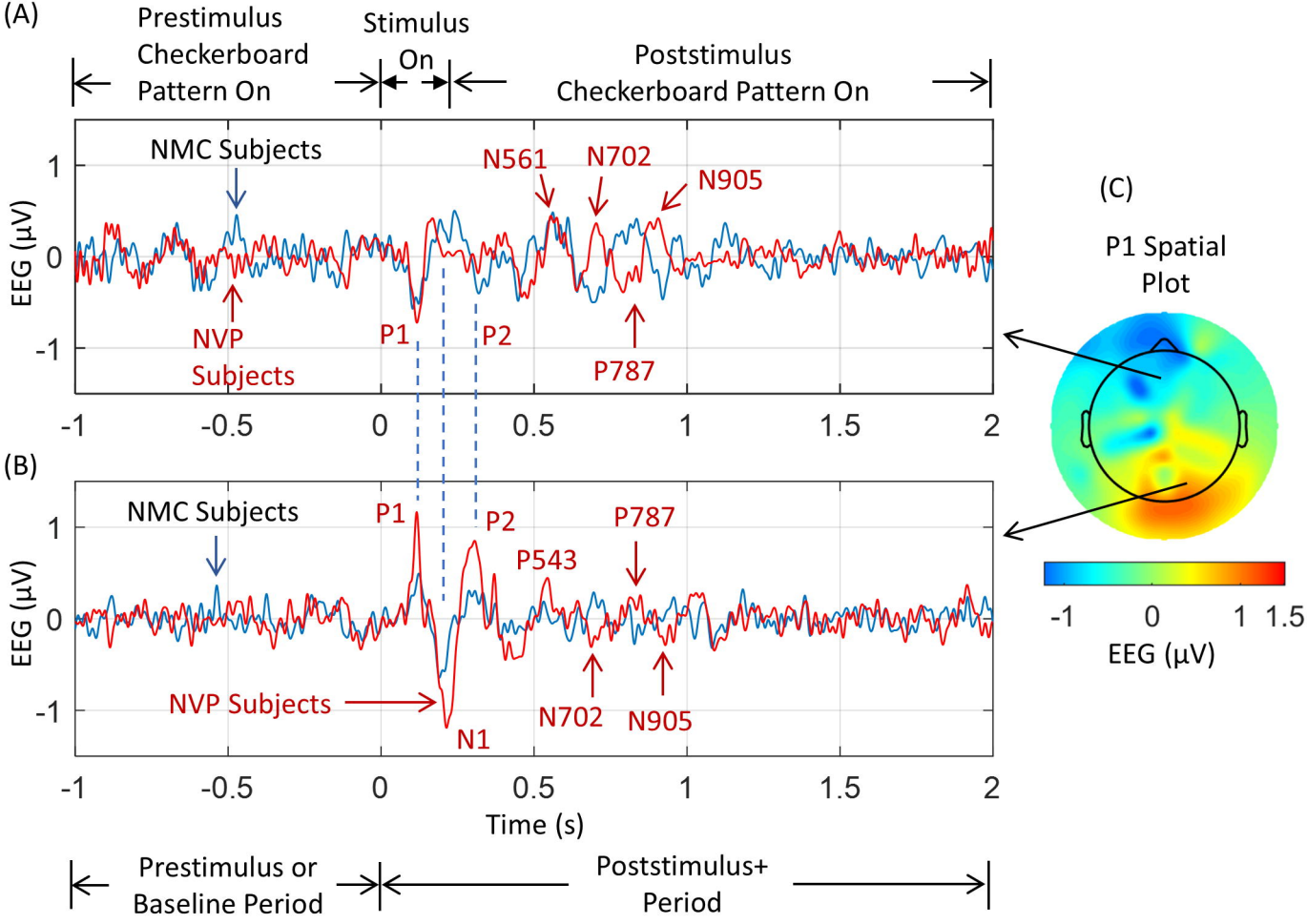
(A)
Prestimulus Checkerboard Pattern On
Stimulus On
Poststimulus Checkerboard Pattern On
NMC Subjects
N561
N702
N905
NVP Subjects
P1
P2
P787
EEG (μV)
(B)
NMC Subjects
P1
P2
P787
P543
NVP Subjects
N1
N702
N905
Time (s)
(C)
P1 Spatial Plot
EEG (μV)
Prestimulus or Baseline Period
Poststimulus+ Period

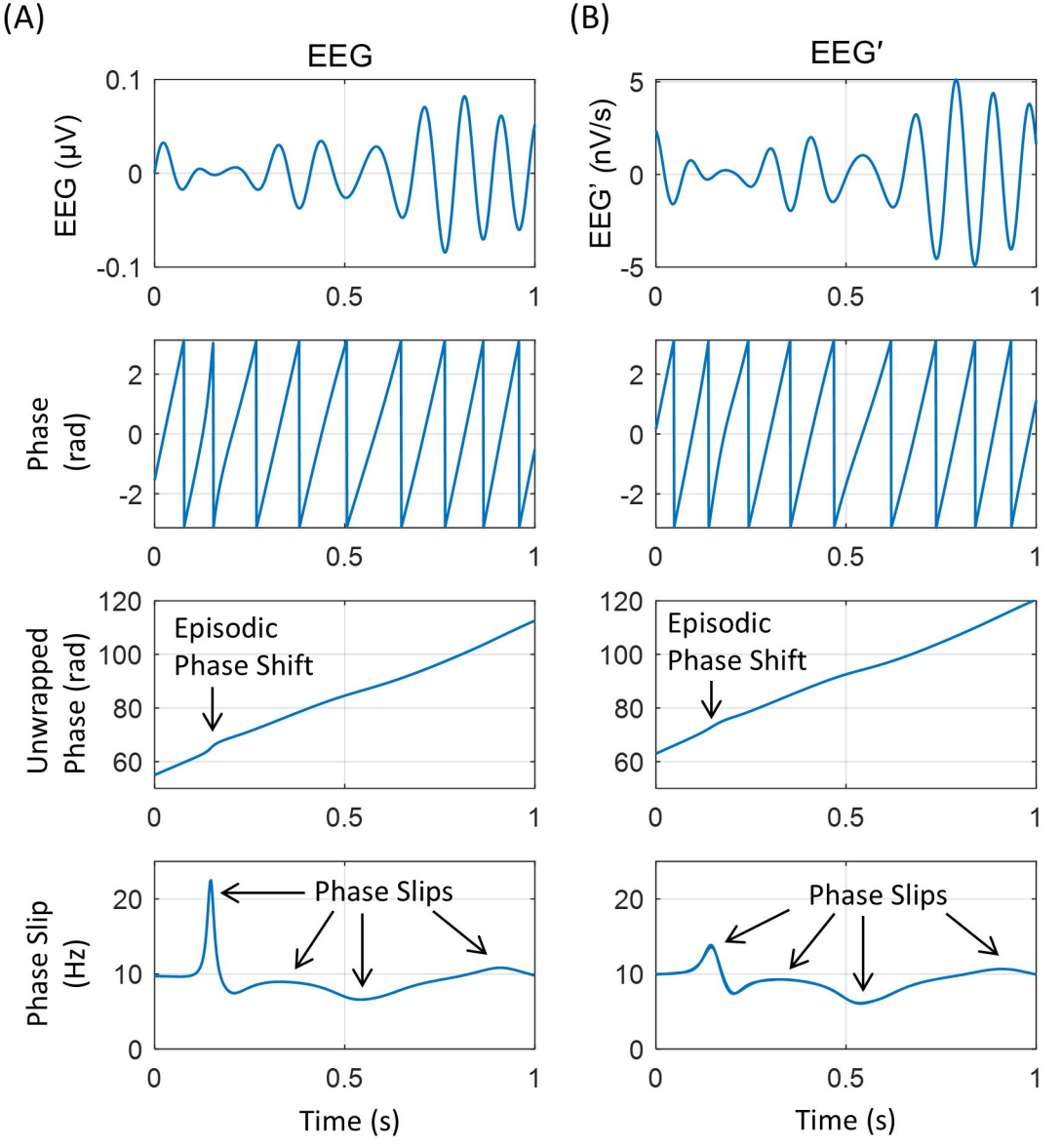
(A)
(B)
EEG
EEG′
EEG (μV)
EEG′ (nV/s)
Phase (rad)
Unwrapped Phase (rad)
Phase Slip (Hz)
Episodic Phase Shift
Phase Slips
Time (s)

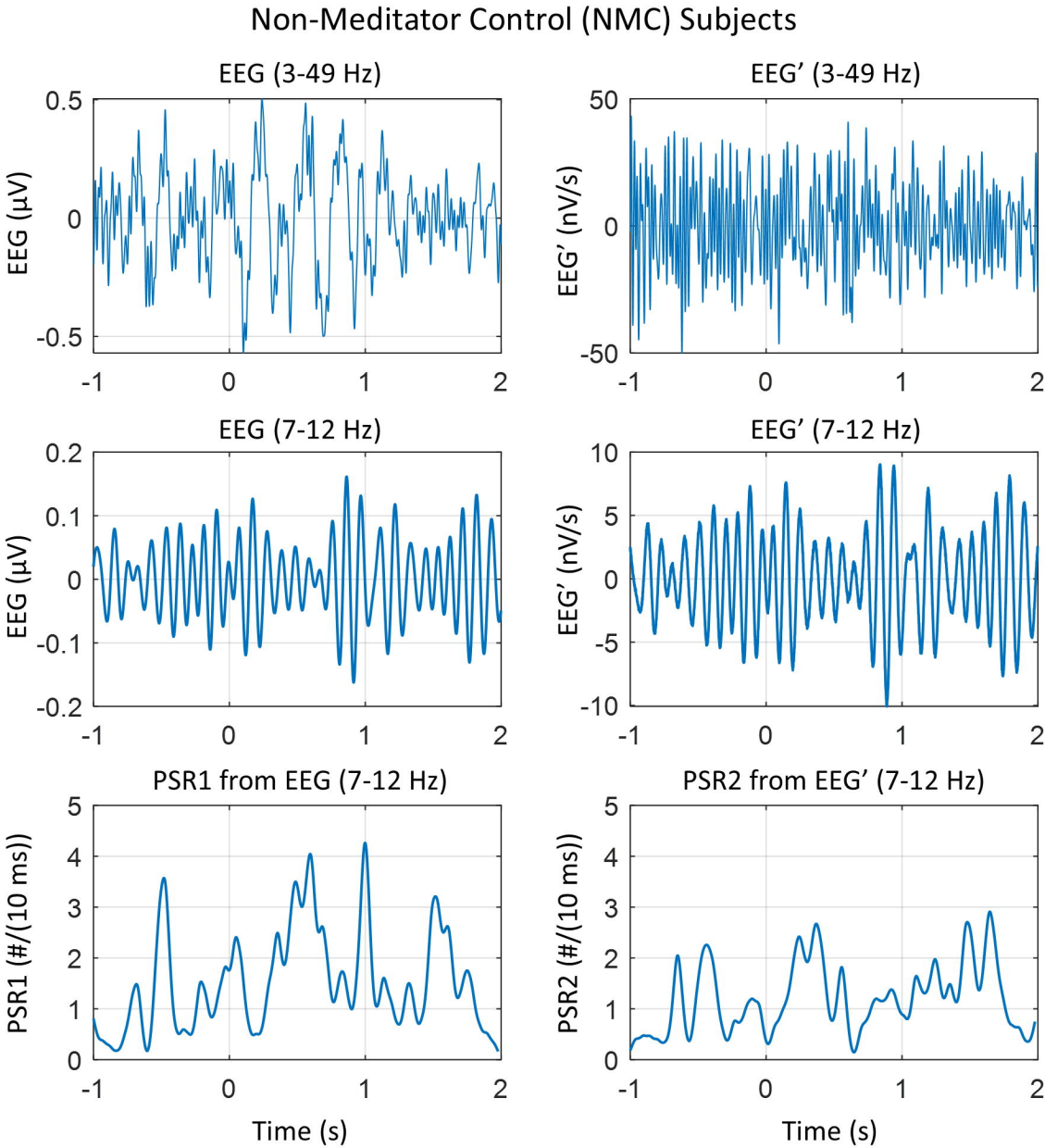
Non-Meditator Control (NMC) Subjects
EEG (3-49 Hz)
EEG (µV)
0.5
0
-0.5
-1
0
1
2
EEG' (3-49 Hz)
EEG' (nV/s)
50
0
-50
EEG (7-12 Hz)
0.2
0.1
-0.1
-0.2
EEG' (7-12 Hz)
10
5
-5
-10
PSR1 from EEG (7-12 Hz)
PSR1 (#/(10 ms))
PSR2 from EEG' (7-12 Hz)
PSR2 (#/(10 ms))
Time (s)

Non-Meditator Control (NMC) Subjects

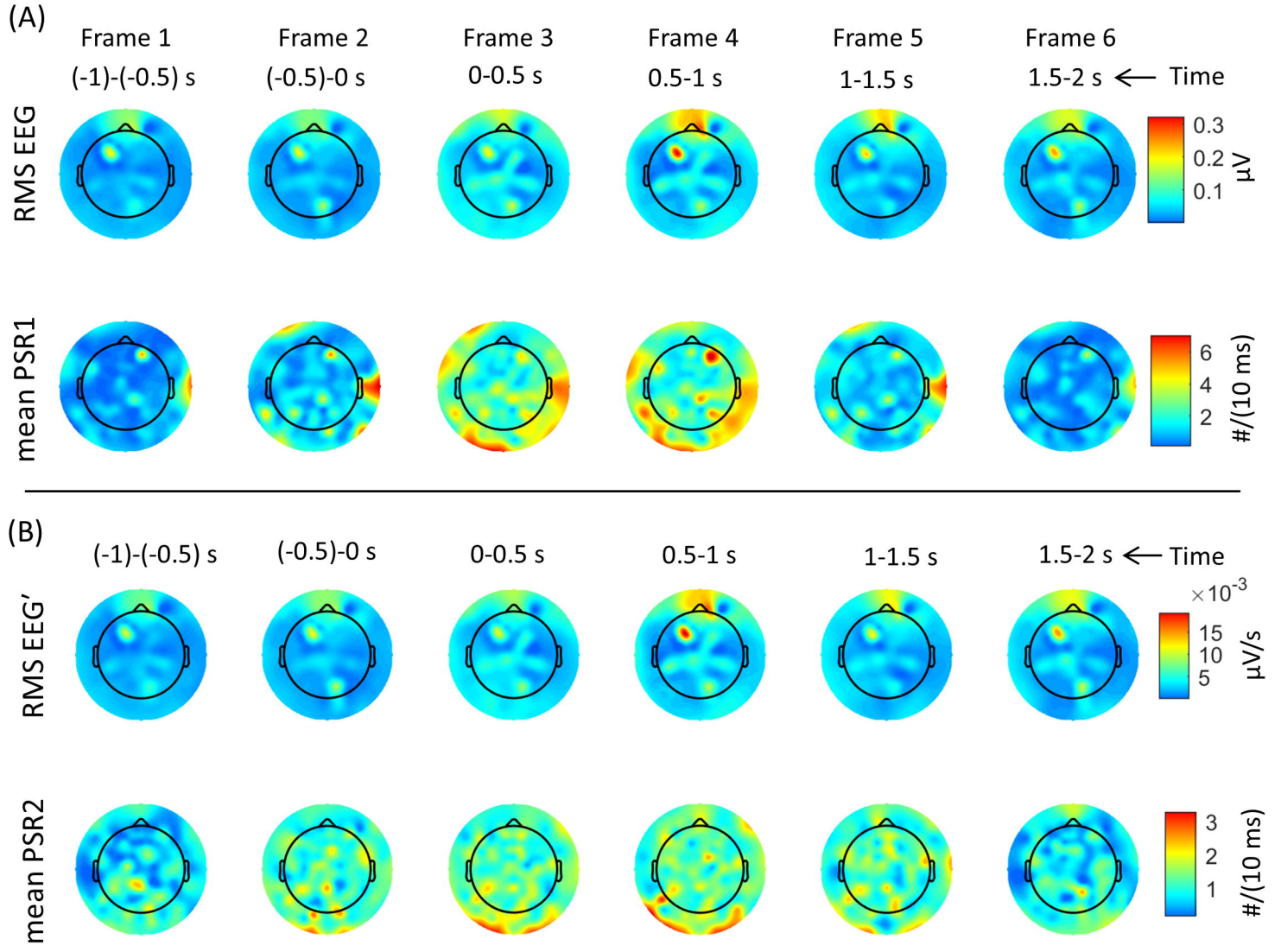

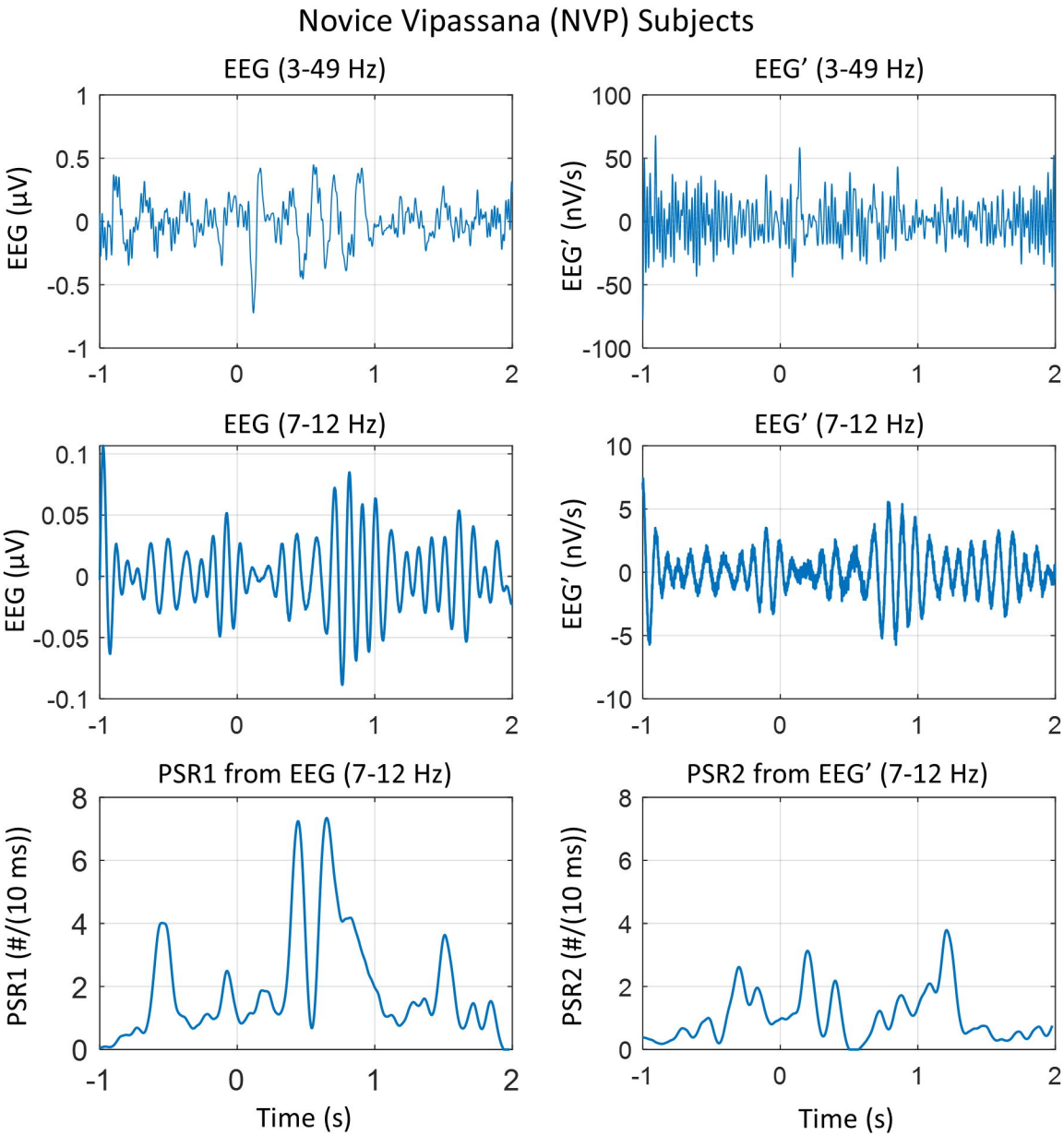
Novice Vipassana (NVP) Subjects
EEG (3-49 Hz)
EEG (μV)
EEG' (3-49 Hz)
EEG' (nV/s)
EEG (7-12 Hz)
EEG (μV)
EEG' (7-12 Hz)
EEG' (nV/s)
PSR1 from EEG (7-12 Hz)
PSR1 (#/(10 ms))
PSR2 from EEG' (7-12 Hz)
PSR2 (#/(10 ms))
Time (s)
Time (s)

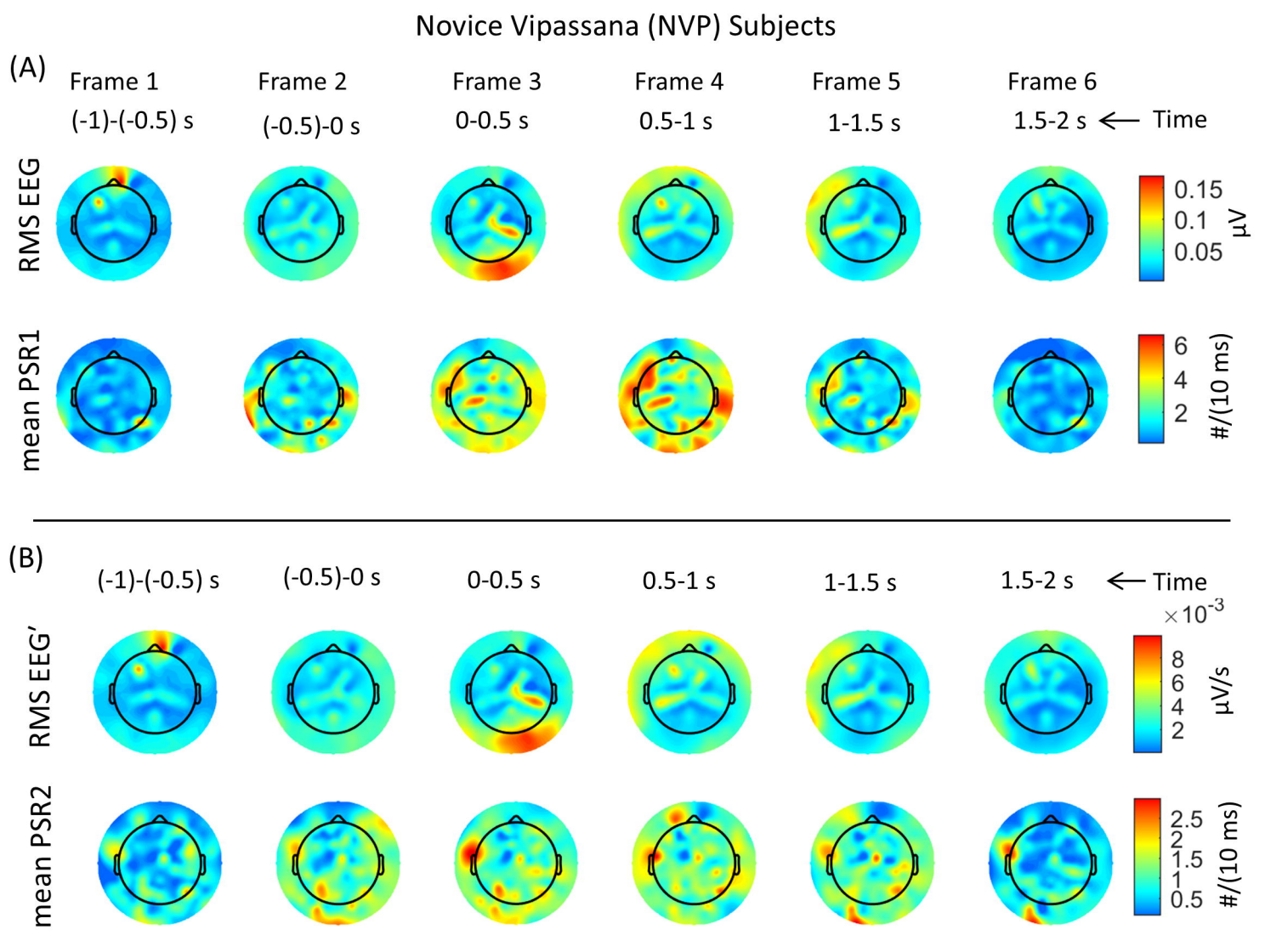
Novice Vipassana (NVP) Subjects
(A)
Frame 1
(-1)-(-0.5) s
Frame 2
(-0.5)-0 s
Frame 3
0-0.5 s
Frame 4
0.5-1 s
Frame 5
1-1.5 s
Frame 6
1.5-2 s
Time
RMS EEG
0.15
0.1
0.05
μV
mean PSR1
6
4
2
#/(10 ms)
(B)
(-1)-(-0.5) s
(-0.5)-0 s
0-0.5 s
0.5-1 s
1-1.5 s
1.5-2 s
Time
RMS EEG'
×10^-3
8
6
4
2
μV/s
mean PSR2
2.5
2
1.5
1
0.5
#/(10 ms)

RMS EEG and Mean PSR1 above Prestimulus Values

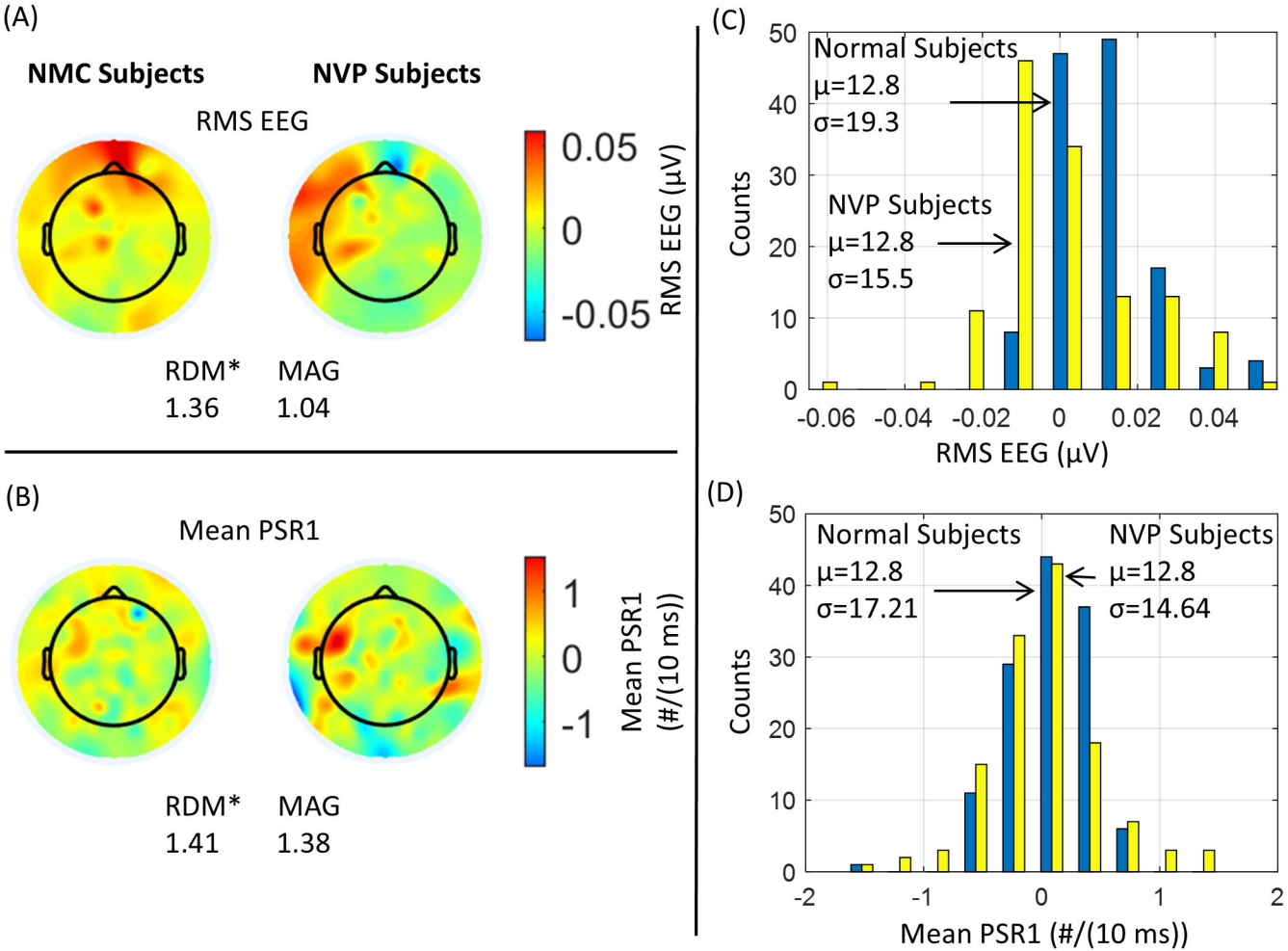

RMS EEG' and Mean PSR2 above Prestimulus Values

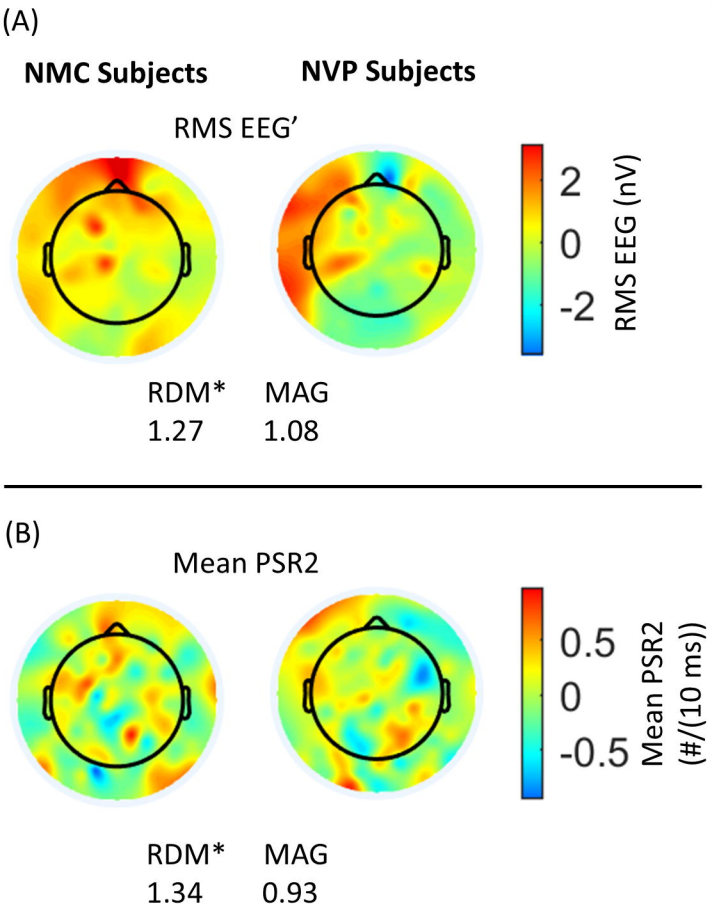

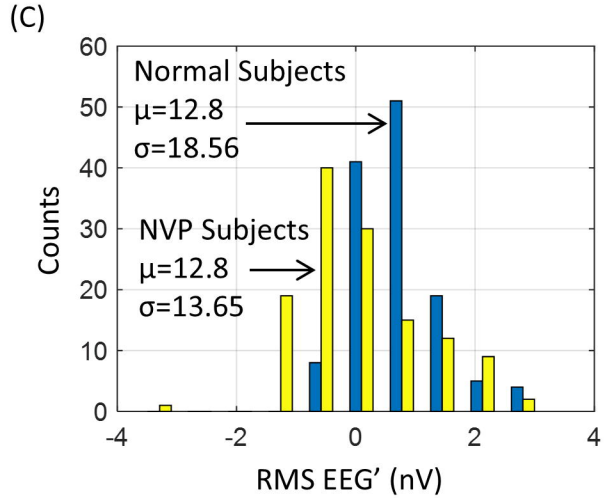

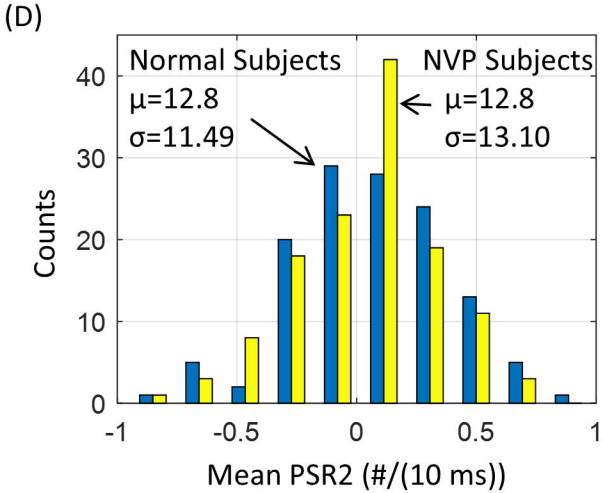

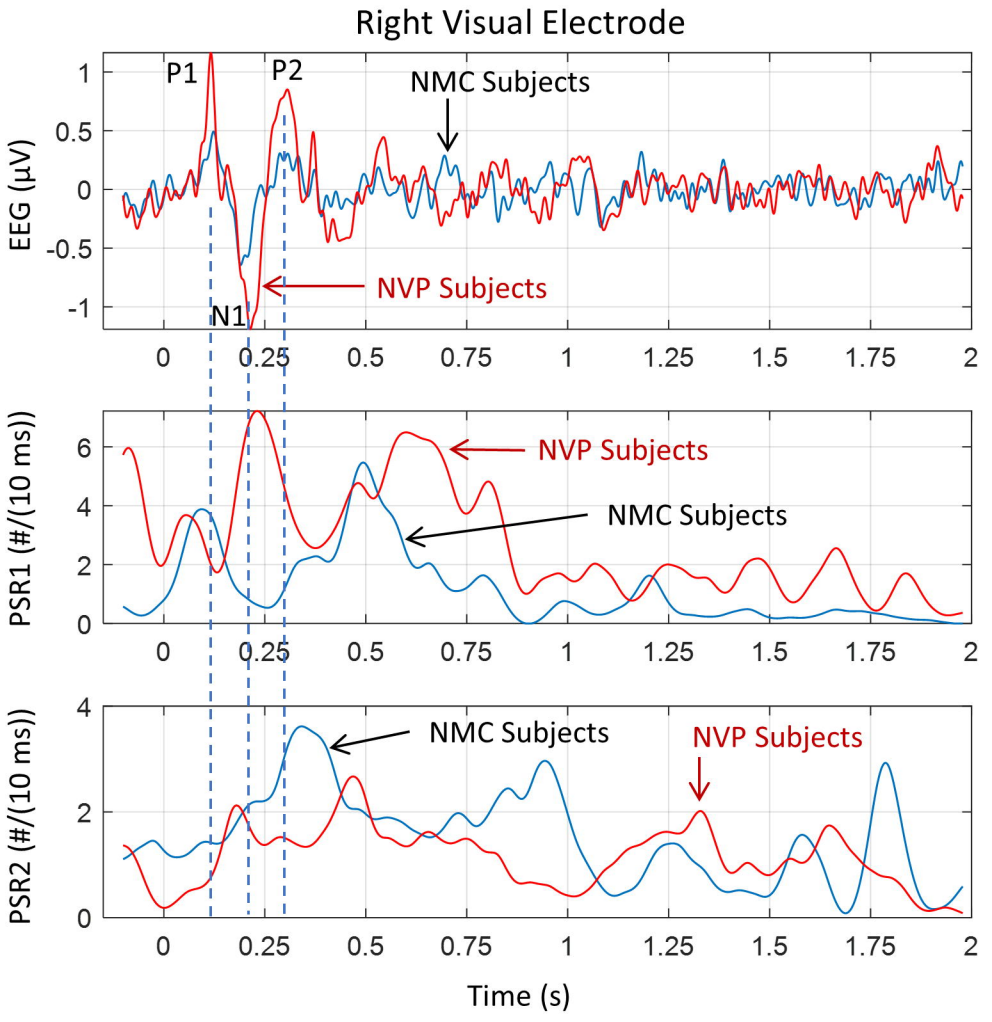
Right Visual Electrode
P1
P2
N1
NMC Subjects
NVP Subjects
EEG (μV)
1
0.5
0
-0.5
-1
0
0.25
0.5
0.75
1
1.25
1.5
1.75
2
PSR1 (#/(10 ms))
6
4
2
0
NVP Subjects
NMC Subjects
PSR2 (#/(10 ms))
4
2
0
NMC Subjects
NVP Subjects
Time (s)

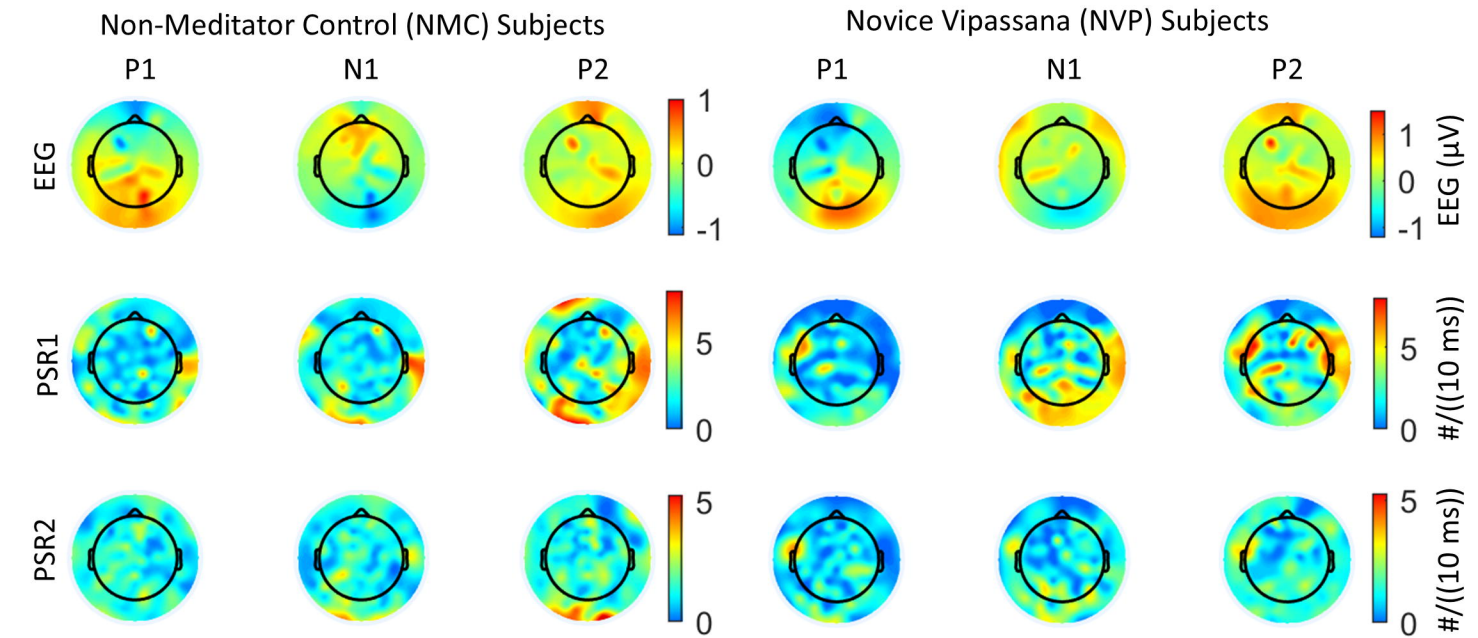
Non-Meditator Control (NMC) Subjects
Novice Vipassana (NVP) Subjects
P1
N1
P2
P1
N1
P2
EEG
PSR1
PSR2
1
0
-1
EEG (μV)
5
0
#/((10 ms))
5
0
#/((10 ms))

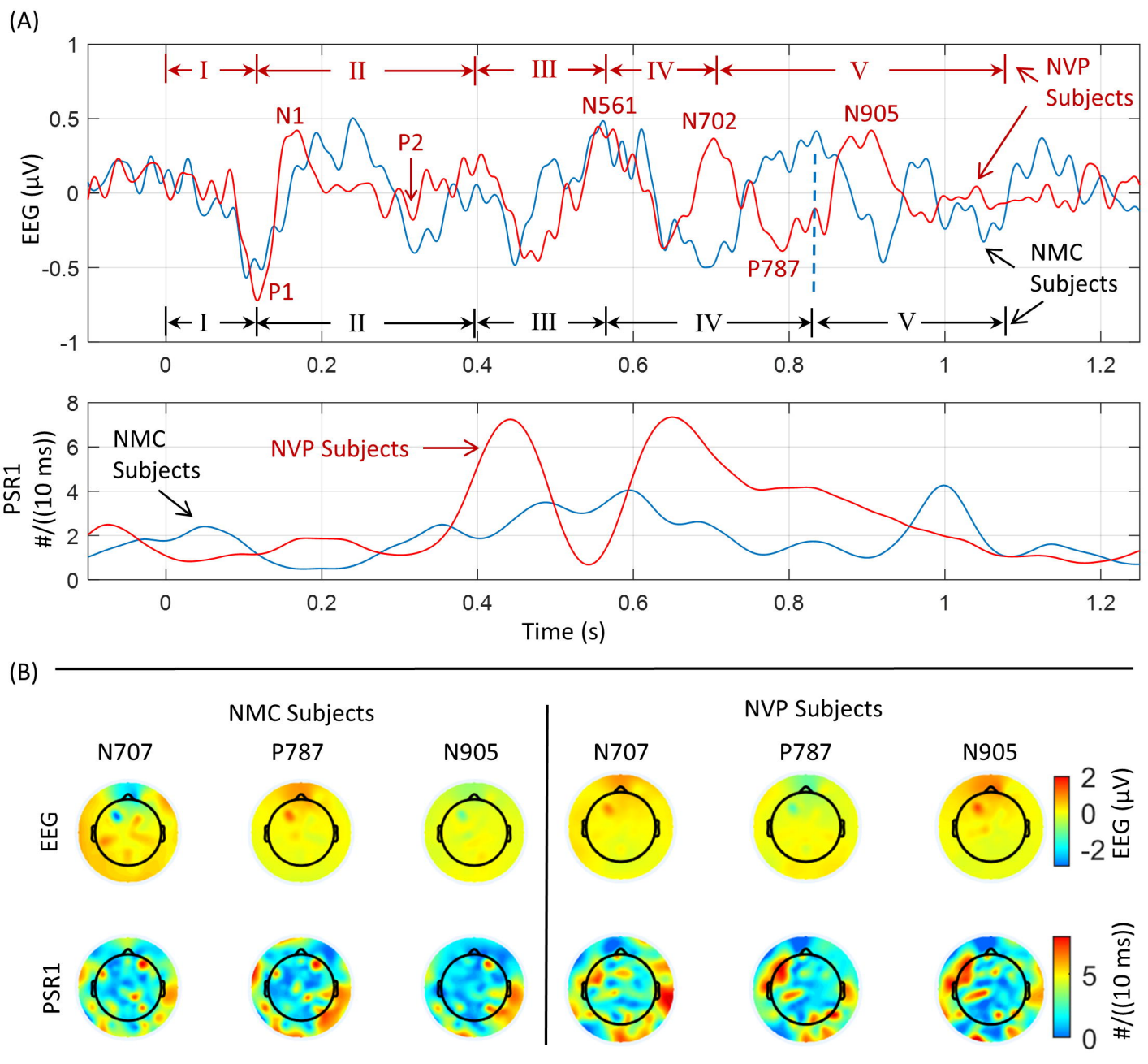
(A)
I
II
III
IV
V
NVP Subjects
N1
P2
N561
N702
N905
P1
P787
NMC Subjects
EEG (μV)
PSR1 #/((10 ms))
NMC Subjects
NVP Subjects
Time (s)
(B)
NMC Subjects
NVP Subjects
N707
P787
N905
EEG
PSR1
EEG (μV)
#/((10 ms))